Journal of proteome research

Article

pubs.acs.org/jpr

Stage Dependence, Cell-Origin Independence, and Prognostic Capacity of Serum Glycan Fucosylation, β1−4 Branching, β1−6 Branching, and α2−6 Sialylation in Cancer

Shadi Ferdosi,[†,‡] Douglas S. Rehder,[‡,○] Paul Maranian,[‡] Erik P. Castle,[§] Thai H. Ho,[∥] Harvey I. Pass,[⊥] Daniel W. Cramer,[#,▽] Karen S. Anderson,[‡] Lei Fu,[○,◆] David E. C. Cole,[○,◆] Tao Le,[¶] Xifeng Wu,[¶] and Chad R. Borges*[,†,‡]

[†]School of Molecular Sciences, Arizona State University, Tempe, Arizona 85287, United States

[‡]Virginia G. Piper Center for Personalized Diagnostics, The Biodesign Institute at Arizona State University, Tempe, Arizona 85287, United States

[§]Department of Urology and [∥]Division of Hematology and Medical Oncology, Mayo Clinic, Phoenix, Arizona 85054, United States

[⊥]Cardiothoracic Surgery, NYU Langone Medical Center, New York, New York 10016, United States

[#]Obstetrics and Gynecology Epidemiology Center, Department of Obstetrics and Gynecology, Brigham and Women's Hospital, Boston, Massachusetts 02115, United States

[▽]Department of Epidemiology, Harvard School of Public Health, Boston, Massachusetts 02115, United States

[○]Department of Clinical Pathology, Sunnybrook Health Sciences Centre, Toronto, Ontario M4N 3M5, Canada

[◆]Department of Laboratory Medicine and Pathobiology, University of Toronto, Toronto, Ontario M5S 1A8, Canada

[¶]University of Texas MD Anderson Cancer Center, Houston, Texas 77030, United States

Supporting Information

ABSTRACT: Glycans represent a promising but only marginally accessed source of cancer markers. We previously reported the development of a molecularly bottom-up approach to plasma and serum (P/S) glycomics based on glycan linkage analysis that captures features such as α2−6 sialylation, β1−6 branching, and core fucosylation as single analytical signals. Based on the behavior of P/S glycans established to date, we hypothesized that the alteration of P/S glycans observed in cancer would be independent of the tissue in which the tumor originated yet exhibit stage dependence that varied little between cancers classified on the basis of tumor origin. Herein, the diagnostic utility of this bottom-up approach as applied to lung cancer patients (n = 127 stage I; n = 20 stage II; n = 81 stage III; and n = 90 stage IV) as well as prostate (n = 40 stage II), serous ovarian (n = 59 stage III), and pancreatic cancer patients (n = 15 rapid autopsy) compared to certifiably healthy individuals (n = 30), nominally healthy individuals (n = 166), and risk-matched controls (n = 300) is reported. Diagnostic performance in lung cancer was stage-dependent, with markers for terminal (total) fucosylation, α2−6 sialylation, β1−4 branching, β1−6 branching, and outer-arm fucosylation most able to differentiate cases from controls. These markers behaved in a similar stage-dependent manner in other types of cancer as well. Notable differences between certifiably healthy individuals and case-matched controls were observed. These markers were not significantly elevated in liver fibrosis. Using a Cox proportional hazards regression model, the marker for α2−6 sialylation was found to predict both progression and survival in lung cancer patients after adjusting for age, gender, smoking status, and stage. The potential mechanistic role of aberrant P/S glycans in cancer progression is discussed.

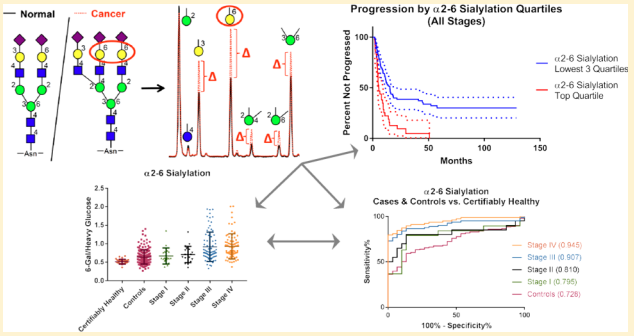

KEYWORDS: *glycans, cancer, plasma, serum, fucosylation, sialylation, branching, smoking, progression, survival*

INTRODUCTION

Serum glycan composition and structure are well-known to be altered in many different types of cancer.[1−4] In fact, for over a decade now, global blood plasma and serum (P/S) glycomics has held out the promise of new, noninvasive cancer markers derived from a small volume of this easily accessible biofluid.[5,6] Modern analytical methods for quantifying the relative abundance of different glycans in P/S vary widely,[7−9] ranging from multiplexed capillary gel electrophoresis with laser-

Received: September 20, 2017
Published: November 12, 2017

DOI: 10.1021/acs.jproteome.7b00672
J. Proteome Res. 2018, 17, 543−558

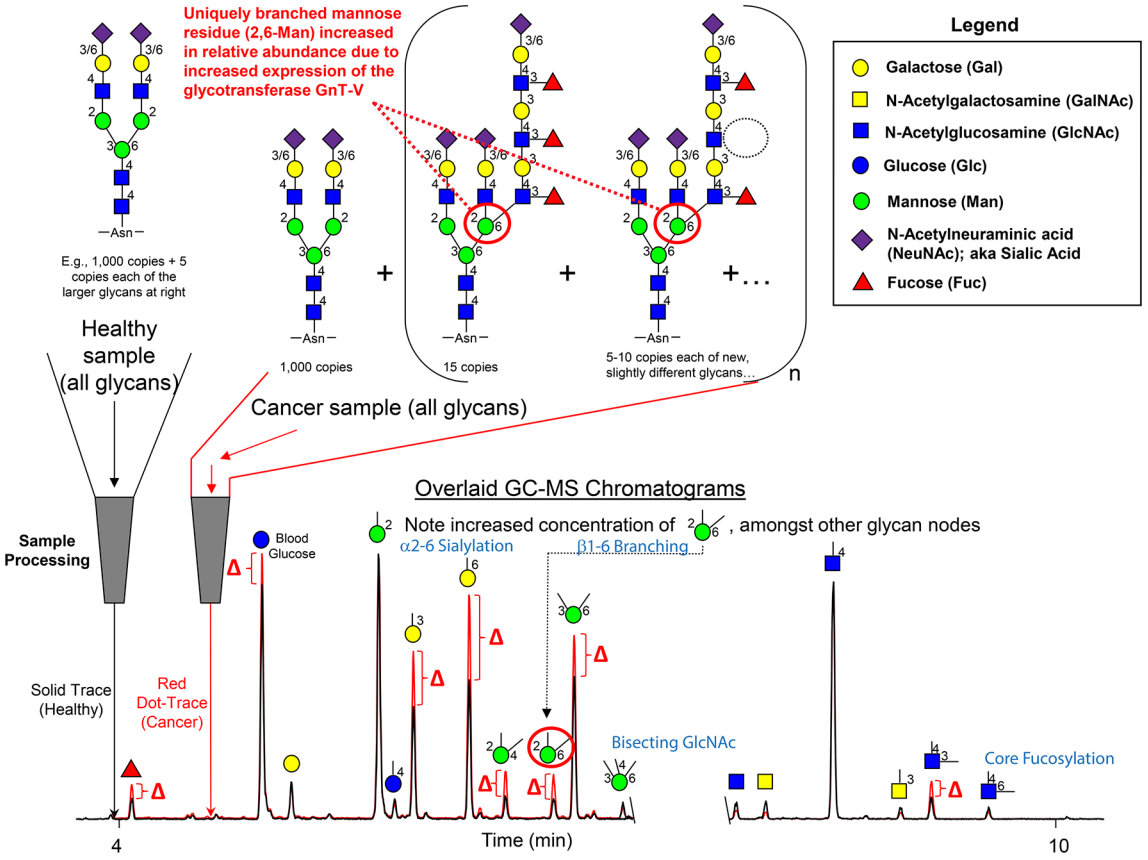

Figure 1. Conceptual overview of the glycan "node" analysis concept, which essentially consists of applying glycan linkage (methylation) analysis to whole biofluids. Intact normal and abnormal glycans including O-glycans, N-glycans, and glycolipids are processed and transformed into partially methylated alditol acetates (PMAAs, Figure 2), each of which corresponds to a particular monosaccharide-and-linkage-specific glycan "node" in the original polymer. As illustrated, analytically pooling together the glycan nodes from among all the aberrant intact glycan structures provides a more-direct surrogate measurement of abnormal glycosyltransferase activity than any individual intact glycan while simultaneously converting unique glycan features such as "core fucosylation", "α2−6 sialylation", "bisecting GlcNAc", and "β1−6 branching" into single analytical signals. Actual extracted ion chromatograms from 9 μL blood plasma samples are shown. Numbers adjacent to monosaccharide residues in glycan structures indicate the position at which the higher residue is linked to the lower residue. This figure was adapted with permission from ref 18. Copyright 2013 American Chemical Society.

induced fluorescence (a DNA sequencer-adapted method)[10,11] to hydrophilic interaction liquid chromatography (HILIC)[12] or porous graphitized carbon (PGC)[13,14] chromatography interfaced with electrospray ionization-based mass spectrometers or as a means of prefractionation prior to analysis by MALDI-MS,[15] for which glycans are generally permethylated prior to analysis.[9,16]

Nearly all approaches employed in P/S glycomics focus on the analysis of intact glycans, most commonly N-linked glycans (generally to the exclusion of O-linked glycans and glycolipids). Quite commonly, accounts of such studies that are focused on cancer conclude by taking a wide-angle view of all intact glycans that were altered in cancer relative to a healthy or benign disease state and reporting unique glycan features such as core fucosylation, bisecting *N*-acetylglucosamine (GlcNAc), and α2−6 sialylation that were found to be increased or decreased in cancer.[6] Often, these features are then directly connected to the activity of specific glycosyltransferases.[17] In 2013, Borges et al.[18] developed a molecularly bottom-up approach to serum glycomics, which, following permethylation of an unfractionated P/S sample, employs the principles of glycan linkage analysis to break down all P/S glycans into monosaccharides in a way that maintains information about which hydroxyl groups of each monosaccharide were connected to other carbohydrate residues in the original glycan polymer[18−20] (Figures 1 and 2). This mode of P/S sample preparation results in a collection of roughly two dozen partially methylated alditol acetates (PMAAs), each of which represents a unique glycan "node" from the original glycan polymers and can readily be quantified by gas chromatography−mass spectrometry (GC−MS). Uniquely, several PMAAs, such as those arising from 2,6-linked mannose, 4,6-linked GlcNAc, and 3,4,6-linked mannose correspond to unique glycan features such as β1−6 branching, core fucosylation, and bisecting GlcNAc, respectively, and capture these unique features as single analytical signals rather than allowing the signal from that feature to be spread across all intact glycans that bear the unique feature (Figure 1). Similarly, many of the PMAAs serve as excellent surrogates for the activities of the glycosyltransferases (GTs) that produced them because only one or two known human GTs are capable of producing that particular glycan monosaccharide linkage pattern.[18] In addition, this unique approach to P/S glycomics simultaneously captures information from all major classes of P/S glycans, including N-, O-, and lipid-linked glycans.[18] The specificity of this approach with regard to producing only those chromatographic peaks for glycan nodes known to be present on a particular preisolated glycoprotein is illustrated within

DOI: 10.1021/acs.jproteome.7b00672
J. Proteome Res. 2018, 17, 543−558

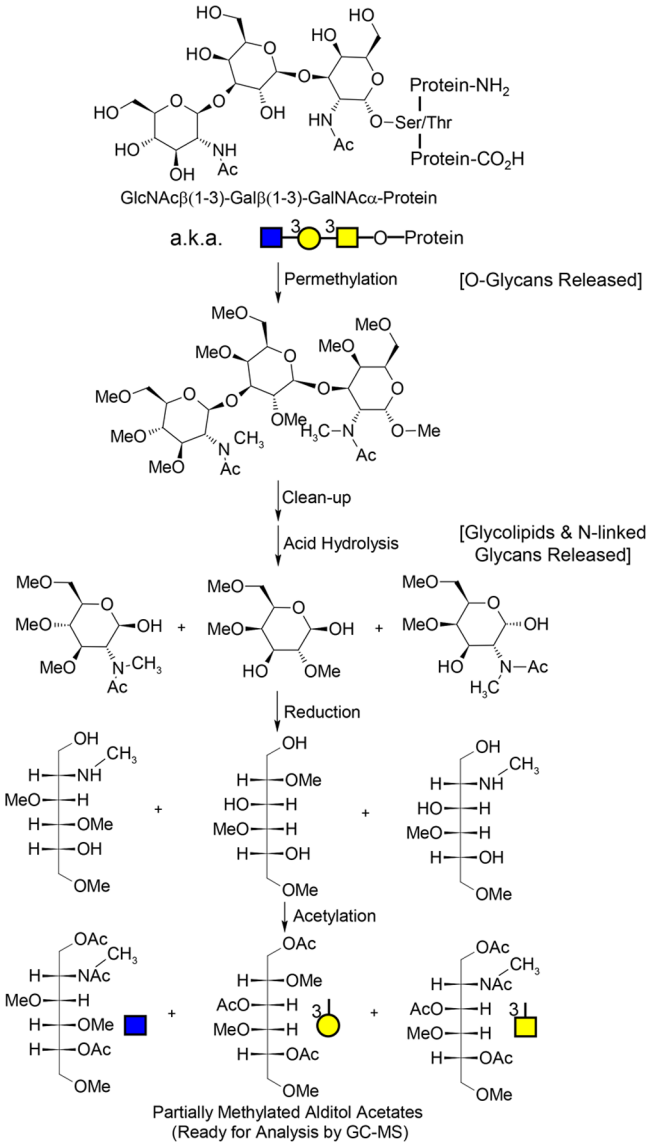

Figure 2. Molecular overview of the glycan "node" analysis procedure. For glycans from blood plasma and other biofluids, O-linked glycans are released during permethylation, while N-linked glycans and glycolipids are released during acid hydrolysis. The unique pattern of methylation and acetylation in the final partially methylated alditol acetates (PMAAs) corresponds to the unique "glycan node" in the original glycan polymer and provides the molecular basis for separation and quantification by GC-MS. Figure adapted with permission from ref 18. Copyright 2013 American Chemical Society.

Figure 3 of the paper in which this approach was originally described.[18]

To date, we have only reported results from pilot studies in which this methodology was applied to (mostly) advanced stages of lung[18] and breast cancer.[20] To gain a representative perspective on the potential utility of this approach to detecting a variety of different types of cancer at varying stages, we have now applied it to over 950 clinical P/S samples from 7 different case control studies across all stages of cancer in which the cancer cases were compared to related benign conditions and healthy controls. A study of plasma samples from 428 Stage I–IV lung cancer patients; age-, gender-, and smoking-status-matched controls; and certifiably healthy living kidney donors serves as the backbone for this report, in which plasma from a single donor served as a quality control specimen in every single batch of samples, facilitating comparisons to pancreatic (rapid autopsy), ovarian (Stage III), prostate (Stage II), and a large independent lung cancer (Stage I) case-control study. Based on the behavior of P/S glycans established to date, we hypothesized that the alteration of P/S glycans observed in cancer would be independent of the tissue in which the tumor originated yet exhibit stage dependence that varied little across cancers classified on the basis of tumor origin.

MATERIALS AND METHODS

Materials

Heavy, stable-isotope-labeled D-glucose (U–$^{13}C_6$, 99%; 1,2,3,4,5,6,6-D7, 97%–98%) was purchased from Cambridge Isotope Laboratories. *N*-Acetyl-D-[UL-$^{13}C_6$]glucosamine was obtained from Omicron Biochemicals, Inc. Methanol was purchased from Honeywell Burdick and Jackson. Acetone was obtained from Avantor Performance Materials. Acetonitrile and dichloromethane were acquired from Fisher Scientific. Chloroform, sodium hydroxide beads (20–40 mesh) DMSO, iodomethane (99%, catalog no. I8507), trifluoroacetic acid (TFA), ammonium hydroxide, sodium borohydride, and acetic anhydride were obtained from Sigma-Aldrich. Pierce spin columns (0.9 mL volume) including plugs were purchased from ThermoFisher Scientific (Waltham, MA, catalog no. 69705). GC–MS autosampler vials and Teflon-lined pierceable caps were acquired from ThermoFisher Scientific. GC consumables were purchased from Agilent; MS consumables were obtained from Waters.

Plasma and Serum Samples

A summary of the case-control sample sets employed in this study is provided in Table 1. All specimens were collected in compliance with the Declaration of Helsinki principles. Once collected, they were coded and de-identified to protect patient identities.

Living Kidney Donors. EDTA plasma samples from certifiably healthy living kidney donors were enrolled in the Multidisciplinary Biobank at Mayo Clinic Arizona under a Mayo Clinic Institutional Review Board (IRB)-approved protocol. Patients eligible for enrollment were those seen at Mayo Clinic Arizona who were ≥18 years old, able to provide informed consent, and undergoing evaluation as a potential living kidney donor. Detailed inclusion and exclusion criteria for these patients are provided in the Supporting Information. None of these patients smoked at the time of health screening and blood collection; 27% were former smokers, and 73% never smoked. Specimens were collected over a 2 year period from December 2013 to December 2015. Standard operating protocols and blood collections were performed as previously described.[21] All specimens were stored at −80 °C prior to shipment to Arizona State University.

Large Lung Cancer Set. Sodium heparin plasma samples for the large lung cancer study were collected at the University of Texas MD Anderson Cancer Center under the supervision of Dr. Xifeng Wu. Heparin is a glycosaminoglycan itself but the vast majority of its monomer units are carboxylated, sulfated, or both. As we have previously described,[18] sulfated and carboxylated glycan monomers cannot be directly detected by the analytical methodology employed in this study. The PMAA from 4-linked GlcNAc could theoretically be produced by the heparin anticoagulant, but empirically, we found in our matched collection studies (described in the Results) that 4-

DOI: 10.1021/acs.jproteome.7b00672
J. Proteome Res. 2018, 17, 543–558

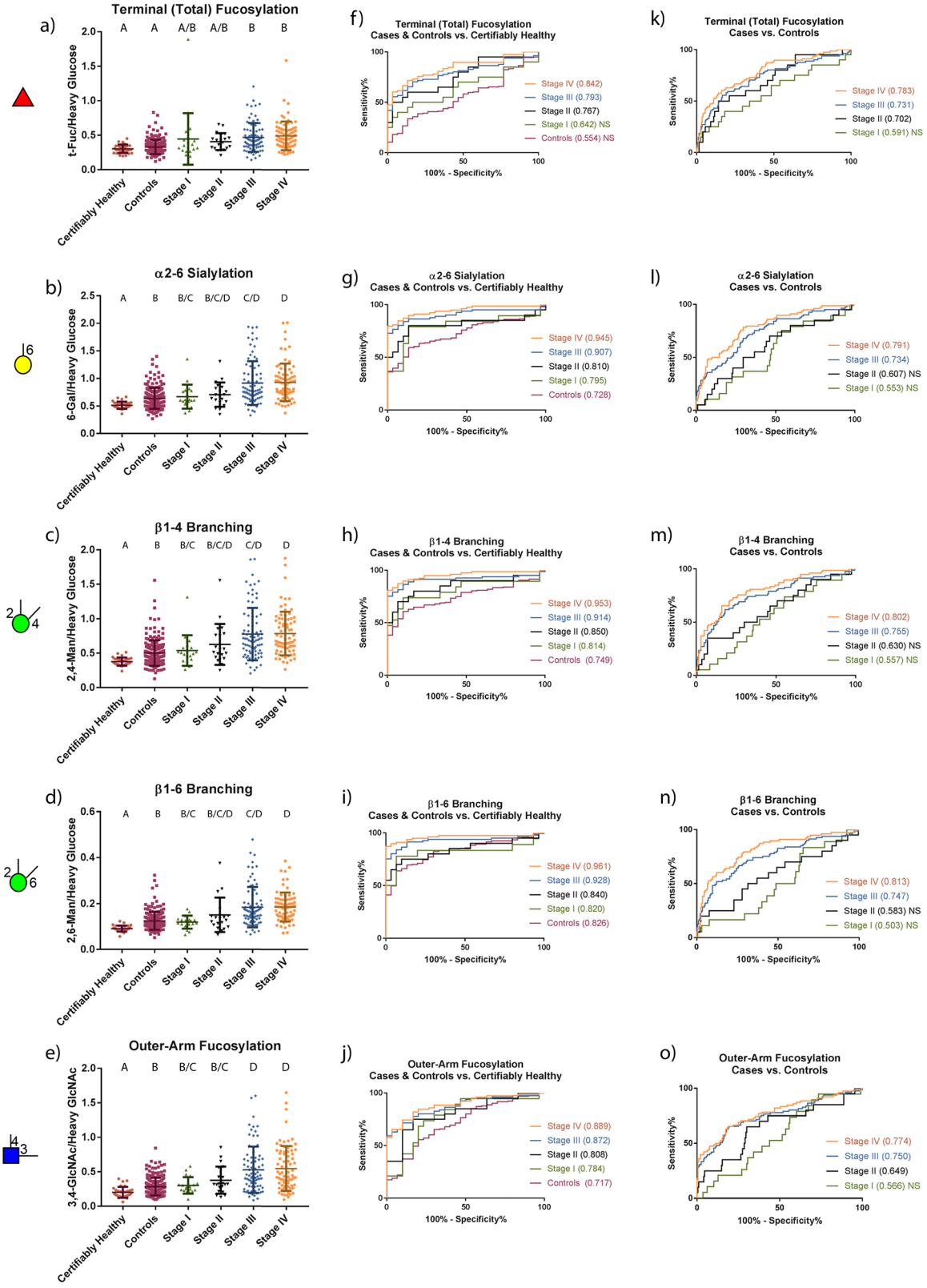

Figure 3. Univariate distributions and associated ROC curves for the top five-performing glycan nodes in the large lung cancer set. The letters above the data points in panels a–e indicate statistically significant differences between the six groups shown; any overlap in lettering between groups indicates a lack of significant difference between the groups (Kruskal–Wallis with Dunn's post hoc test). ROC curves for lung cancer cases (separated by stage) and controls vs certifiably healthy patients are shown in panels f–j; stage I–IV cancer patients vs controls are shown in panels k–o. ROC curve AUCs are provided in parentheses next to the specified stages. "NS" next to ROC curve AUCs indicates that the ROC curve does not show a statistically significant difference between the two groups being compared. Glycan node symbol definitions are the same as in Figure 1.

DOI: 10.1021/acs.jproteome.7b00672
J. Proteome Res. 2018, 17, 543–558

Table 1. Composition of Sample Sets and Their Sub-Cohorts

name of sample set	serum or type of plasma	certifiably healthy	nominally healthy[a]	controls[b]	Stage I	Stage II	Stage III	Stage IV	rapid autopsy
living kidney donors	EDTA plasma	30[c]	–	–	–	–	–	–	–
large lung cancer	heparin plasma[d]	–	–	199	20	20	81	78	–
liver fibrosis (not cancer)	serum	–	–	13	9	7	2	2	–
Stage I lung adenocarcinoma	serum	–	–	73	107	–	–	–	–
Stage II prostate cancer	serum	–	56	–	–	40	–	–	–
Stage III serous ovarian cancer	serum	–	87	–	–	–	59	–	–
Stage IV lung cancer	serum	–	23	–	–	–	–	12	–
rapid autopsy pancreatic cancer	serum	–	–	15	–	–	–	–	15

[a]Nominally healthy donors were self-reported as healthy and were only age- and gender-matched to cases. [b]Age- and gender-matched to cases; smoking-status-matched in lung cancer sets; benign nodule positive in the Stage I lung adenocarcinoma set; benign inflammatory condition-matched in the pancreatic cancer set. [c]These samples were analyzed immediately prior to, but in a separate set of batches from, the large lung cancer set. Results for the quality control specimens analyzed in both sets of batches were not significantly different from one another. [d]Heparin is a glycosaminoglycan, but for reasons explained in the Materials and Methods section, it does not impact the results of glycan node analysis.

linked GlcNAc from heparin plasma is not significantly different from EDTA plasma or serum. Specimens for lung cancer cases and controls from the University of Texas MD Anderson Cancer Center included in this study are part of an ongoing large lung cancer study that has been recruiting since 1995. This study has received approval from the University of Texas MD Anderson Cancer Center and Kelsey–Seybold institutional review boards. Venous blood was drawn from newly diagnosed and histologically confirmed lung cancer patients (prior to therapy) and age-, gender-, and ethnicity-matched controls at the MD Anderson Cancer Center hospital and the nearby Kelsey–Seybold Clinic, respectively. All blood was drawn and processed under the same SOP. Patients were not necessarily in a fasted state. Blood was centrifuged then aliquoted and placed into a liquid nitrogen tank. After collection, samples were coded and de-identified prior to shipment to Arizona State University for analysis. A more-detailed profile of the clinical characteristics of the patients in this large lung cancer study is provided in Table S1.

Liver Fibrosis (Non-Cancerous). Serum samples from patients at all stages of liver fibrosis were collected at the Sunnybrook Health Sciences Centre, under the direction of Dr. Lei Fu and Dr. David E. C. Cole. This study was approved by Research Ethics Board, Sunnybrook Health Sciences Centre, Toronto. Patients were recruited between 2007 and 2011. Written informed consent was obtained from each participant. All subjects with various chronic liver diseases were considered eligible if they would have liver biopsy for the diagnosis of liver fibrosis as part of their routine care. Blood specimens were collected, and serum was separated from cells following standard clinical laboratory procedures. Serum aliquots were stored in −70 °C. The specimens were coded and de-identified according to the study protocol.

Stage I Lung Adenocarcinoma. Serum samples from stage I lung adenocarcinoma patients and age-, gender-, and smoking-status-matched controls were collected under NYU IRB approval at the NYU Langone Medical Center by Dr. Harvey Pass. Arterial blood samples were collected from fasting patients undergoing surgery in the time frame from September 2006 to August 2013 to remove one or more lung nodules that were detected during a CT scan. Determination of whether nodules were benign or malignant was made following a pathological exam of the excised nodules. Serum was collected in standard glass serum tubes and allowed to sit upright for 30–60 min to allow clotting. Subsequently, tubes were centrifuged at 1200*g* for 20 min at room temperature, then aliquoted and placed at −80 °C within 2–3 h of collection. No freeze–thaw cycles occurred prior to shipment to Arizona State University (Borges lab) for analysis.

Stage II Prostate Cancer. Serum samples from stage II prostate cancer patients were obtained from the Cooperative Human Tissue Network (CHTN), an NIH-sponsored biospecimen collection agency. The quality management system of the CHTN is described elsewhere.[22] Age-matched control samples from nominally healthy male donors were obtained from ProMedDx (Norton, MA).

Stage III Serous Ovarian Cancer. Serum specimens from stage III serous ovarian cancer patients were collected at Brigham and Women's Hospital under IRB approval by Dr. Daniel Cramer. Sera were obtained at the time of presentation prior to surgery. Age, gender, and location matched control sera from women without a history of cancer (other than nonmelanoma skin cancer) were obtained from the general population under a standardized serum collection protocol. All serum samples were collected from 2001 to 2010 and were stored at −80 °C prior to analysis. These specimens have previously been described.[23,24]

Stage IV Lung Cancer. A set of serum samples from stage IV lung cancer patients and age- and gender-matched nominally healthy control donors that was completely separate from those provided by Dr. Xifeng Wu at the University of Texas MD Anderson Cancer Center was obtained from ProMedDx.

Rapid Autopsy Pancreatic Cancer. Serum specimens from rapid autopsy patients who had recently died from pancreatic cancer were collected by Dr. Michael Hollingsworth at the University of Nebraska Medical Center under IRB approval. These samples have previously been described.[25] In brief, specimens were collected within 2–3 h of death. Control serum samples were from patients with benign pancreatic conditions and elevated CA19–9 levels. Samples were coded, de-identified, and kept at −80 °C prior to shipment to Arizona State University.

Additional Biospecimen Details. As described above, all blood samples were processed into P/S immediately following collection and stored at −70 °C or colder until analyzed. Following shipment in dry ice, vial headspace was vented prior to thawing to avoid CO_2-mediated sample acidification.[26] The molecular integrity of the sample set that showed the greatest differences between cases and controls (rapid autopsy pancreatic cancer sera) was examined using an assay based

DOI: 10.1021/acs.jproteome.7b00672
J. Proteome Res. 2018, 17, 543–558

on ex vivo protein oxidation that was recently developed by the Borges group.[27] The prostate cancer and stage I lung adenocarcinoma sets were spot-checked as well. No samples produced evidence for concern about specimen integrity.

In this study, multiple independent sets of sample were compared to each other. Each case-control set was analyzed blind and in random order. Within each batch, across all sets, a quality control (QC) EDTA plasma sample was included consisting of a 9 uL aliquot of the same bulk plasma sample to verify the reproducibility across batches. Notably, the samples from the certifiably healthy living kidney donors were analyzed in separate batches of samples from those in the large lung cancer set. To justify direct comparison of these two sets of samples, we verified that the average values measured for each glycan node in the two sets of QC sample results were not statistically significantly different. Moreover, if the average value of the QC sample was slightly higher or lower in the large lung cancer set relative to the living kidney donor set a scaling factor based on this difference in QC samples was employed to adjust the living kidney donor data set. For each glycan node, this adjustment brought the living kidney donor data set distribution slightly closer to the control distributions observed in the large lung cancer set, meaning that it was a conservative adjustment. Furthermore, to validate the comparability of results in serum and multiple different types of plasma, the glycan "node" analysis procedure was applied to matched sets of P/S samples from 21 donors. This set consisted of four different types of plasma and a serum sample from each donor. The difference between these four types of plasma was based on the different anticoagulants, which were K_2EDTA, K_3EDTA, sodium EDTA, and 3.8% sodium citrate. In an additional study, six matched-collection aliquots of serum, K_2EDTA plasma, and heparin plasma from a single donor were analyzed and compared to each other to verify the consistency of glycan nodes between the aforementioned types of samples.

Experimental Procedures

The global glycan methylation analysis procedure consisted of five main steps; permethylation, trifluoroacetic acid (TFA) hydrolysis, reduction of sugar aldehydes, acetylation of nascent hydroxyl groups, and final cleanup.[18,19] Each step is described in detail in the following.

Permethylation, Nonreductive Release, and Purification of Glycans. A total of 9 μL of P/S was added into a 1.5 mL eppendorf tube followed by 1 μL of a 10 mM solution of heavy-labeled D-glucose (U-$^{13}C_6$, 99%; 1,2,3,4,5,6,6-D7, 97%–98%), and N-acetyl-D-[UL-$^{13}C_6$]glucosamine, which served as internal standards for relative quantification. Then, 270 μL of dimethyl sulfoxide (DMSO) was added to the biological sample and mixed to dissolve completely. Once the sample was fully dissolved, 105 μL of iodomethane was added to the mixture. This solution was then added to a plugged 1 mL spin column, which contained ~0.7 g of sodium hydroxide beads. The NaOH beads had been preconditioned with acetonitrile and rinsed with DMSO twice before the sample was added. Then, the NaOH column was stirred occasionally for 11 min. When finished, samples were unplugged and spun for 15 s at 5000 rpm (2400g) in a microcentrifuge to extract the glycan-containing solution. To wash off all the permethylated glycan, 300 μL of acetonitrile was added to the spin column and then centrifuged for 30 s at 10 000 rpm (9600g). Then, samples from the first spin-through were placed in a silanized 13 × 100 mm glass test tube containing approximately 3.5 mL of 0.5 M NaCl solution in 0.2 M sodium phosphate buffer (pH 7.0) and mixed well. Next, the second spin-through was pooled with the rest of the sample, avoiding the white residue at the bottom of the spin column. The test tube was capped and shaken thoroughly after adding 1.2 mL of chloroform to the sample. Liquid/liquid extraction was performed three times, saving the chloroform layer. The chloroform layer was then extracted with a silanized pipet, transferred to a silanized glass test tube, and dried under nitrogen at heater-block temperature setting of 74 °C.

TFA Hydrolysis. A total of 325 μL of 2 M TFA was added to each sample. Samples were then capped and heated at 121 °C for 2 h. Afterward, samples were dried down under nitrogen at 74 °C.

Reduction of Sugar Aldehydes. A total of 475 μL of a freshly prepared 10 mg/mL solution of sodium borohydride in 1 M ammonium hydroxide was added to each test tube. After the sample was allowed to react for 1 h at room temperature, 63 μL of methanol was added to each sample and then dried down at 74 °C under nitrogen. A solution of 9:1 (v/v) methanol/acetic acid was then prepared, and 125 μL was added to each test tube, which was again dried under nitrogen. Before moving forward, the samples were fully dried in a vacuum desiccator for at least 15–20 min.

Acetylation of Nascent Hydroxyl Groups. A total of 18 μL of water was added to each sample and mixed well to dissolve the entire sample residue. A total of 250 μL of acetic anhydride was then added to each sample. Next, the sample was sonicated in a water bath for 2 min, followed by an incubation for 10 min at 60 °C. A total of 230 μL of concentrated TFA was then added to each test tube. The capped test tube was then incubated at 60 °C for 10 min.

Final Cleanup. Approximately 2 mL of methylene chloride was added to each test tube and mixed well. Then, 2 mL water was added to each sample and mixed well. Liquid/liquid extraction was performed twice, saving the organic layer. Next, the organic layer was transferred with a silanized glass pipet into a silanized autosampler vial. The organic layer was then evaporated under nitrogen, reconstituted in 120 μL of acetone and capped for injection onto GC–MS. A molecular overview of the global glycan methylation analysis procedure is shown in Figure 2.

Gas Chromatography–Mass Spectrometry. For sample analysis, an Agilent Model A7890 gas chromatograph (equipped with a CTC PAL autosampler) was used coupled to a Waters GCT (time-of-flight) mass spectrometer. A total of 1 μL of the sample was injected in split mode onto an Agilent split-mode liner that contained a small plug of silanized glass wool with the temperature set to 280 °C. For all samples, one injection was made at split ratio of 20:1. A 30 m DB-5 ms GC column was used for chromatography. The oven temperature was initially held at 165 °C for 0.5 min. Then, the temperature increased 10 °C/min up to 265 °C, followed by an immediate increase of 30 °C/min to 325 °C, where it was kept constant for 3 min. The total run time was 15.5 min. The temperature of the transfer line was kept at 250 °C. After the sample components were eluted from the GC column, they were subjected to electron ionization with an electron energy of 70 eV at a temperature of 250 °C. The m/z range of analysis was 40–800 with a spectral acquisition rate of 10 Hz. Perfluorotributylamine was used for the daily tuning and calibration of the mass spectrometer.

DOI: 10.1021/acs.jproteome.7b00672
J. Proteome Res. 2018, 17, 543–558

Table 2. Statistically Significant Differences between Cohorts within the Large Lung Cancer Study[a]

glycan node[b]	CH vs C	CH vs I	CH vs II	CH vs III	CH vs IV	C vs I	C vs II	C vs III	C vs IV	I vs II	I vs III	I vs IV	II vs III	II vs IV	III vs IV
t-Fucose	ns	ii	ns	iiii	iiii	ii	ns	iiii	iiii	ns	ns	ns	ns	ns	ns
t-Gal	ns	ns	ns	i	iii	ns	ns	iii	iiii	ns	ns	ns	ns	ns	ns
2-Man	ns	ii	i	iiii	iiii	i	ns	iiii	iiii	ns	ns	ns	ns	ns	ns
4-Glc	dddd	dd	dddd	dddd	dddd	ii	ns	i	i	ns	ns	ns	ns	ns	ns
3-Gal	ns	ns	ns	i	i	ns	ns	i	i	ns	ns	ns	ns	ns	ns
6-Gal	i	ns	i	iiii	iiii	ns	ns	iiii	iiii	ns	iii	iii	ii	ii	ns
3,4-Gal	ns	ns	iiii	ns	ns	ns	iiii	i	i	iii	ns	ns	ii	ii	ns
2,4-Man	i	i	ii	iiii	iiii	ns	ns	iiii	iiii	ns	iii	iii	i	i	ns
2,6-Man	ii	i	iii	iiii	iiii	ns	ns	iiii	iiii	ns	iii	iii	i	i	ns
3,6-Man	ns	ns	ns	iii	iii	ns	ns	iiii	iiii	ns	ns	ns	ns	ns	ns
3,6-Gal	ns	ns	ns	ns	ns	ns	ns	ns	ns	ns	ns	ns	ns	ns	ns
3,4,6-Man	i	iiii	i	ii	ii	ii	ns	ns	ns	ns	i	i	ns	ns	ns
t-GlcNAc	ns	ns	i	iiii	iiii	ns	i	iiii	iiii	ns	ii	i	ns	ns	ns
4-GlcNAc	i	ns	i	iiii	iiii	ns	ns	iiii	iiii	ns	ii	ii	ns	i	ns
3-GlcNAc	ns	ns	i	iiii	iiii	ns	ns	iiii	iiii	ns	iii	iii	ns	ns	ns
3-GalNAc	ii	ns	i	iiii	iiii	ns	ns	ii	iii	ns	ii	iii	ns	ii	ns
3,4-GlcNAc	ns	ns	i	iiii	iiii	ns	ns	iiii	iiii	ns	iii	iii	i	ii	ns
4,6-GlcNAc	ii	ns	ii	iiii	iiii	ns	ns	iii	iii	ns	ii	ii	ns	ns	ns
3,6-GalNAc	iiii	iii	iii	iiii	iiii	ns	ns	ii	iii	ns	ns	ns	ns	ns	ns

[a]Hexose data were normalized to heavy, stable isotope labeled glucose (Glc) and HexNAc data normalized to heavy, stable isotope labeled GlcNAc. [b]Kruskal–Wallis test followed by Benjamini–Hochberg false discovery correction procedure where significance at the 95% confidence level is given by $p < 0.05$. "ns" indicates "not significant". "i" and "d" stand for "increased" or "decreased" in the clinically more advanced cohort listed in the column header. "i" or "d" indicates $p < 0.05$, "ii" or "dd" indicates $p < 0.01$, "iii" or "ddd" indicates $p < 0.001$, and "iiii" and "dddd" indicates $p < 0.0001$. CH: certifiably healthy; C: controls; I: Stage I; II: Stage II; III: Stage III; and IV: Stage IV.

Data Processing

Quantification was done by integrating the summed extracted ion chromatogram peak areas (details provided elsewhere)[18] using QuanLynx software. The peaks were integrated automatically and verified manually. Then, all the information given by integration was exported to a spreadsheet for further analysis.

Statistical Analysis

All data (chromatographic peak areas) for each sample analyzed as part of this study are provided within a spreadsheet available as the Supporting Information. The peak area for each glycan node was normalized in one of two possible ways. In the first approach, individual hexoses were normalized to heavy glucose, and individual HexNAcs were normalized to heavy *N*-acetyl glucosamine (heavy GlcNAc). (Notably, these two internal standards were omitted during analysis of the prostate cancer set of samples.) In the second approach, individual hexoses were normalized to the sum of all endogenous hexoses, and individual HexNAcs were normalized to the sum of all endogenous HexNAcs. This normalization scheme provided modestly improved within-batch reproducibility but limited observation of potential simultaneous increases in all glycan nodes; see the spreadsheet provided in the Supporting Information "Average CVs" worksheet for details on the reproducibility of each normalization approach. Based on the QC sample analyzed in each batch, the average percent CV for the heavy glucose/heavy GlcNAc normalization approach for the top five performing glycan nodes described in the Results section was 17%; for normalization by the sum of endogenous hexoses or HexNAcs, this value was 10%.

Each stage of each cohort was log-transformed, and outliers were removed with the ROUT method at Q = 1% using GraphPad Prism 7. Data were then reversed transformed by taking the anti-log of each value. Differences between patient cohorts and stages in the large lung cancer study were evaluated by means of the Kruskal–Wallis test followed by the Benjamini–Hochberg false discovery correction procedure using R version 3.3.3. This software was also used to generate the receiver operating characteristic (ROC) curves that were statistically compared to one another via DeLong's test using RStudio Version 1.0.143. GraphPad Prism 7 was used to plot the ROC curves shown in Figures 3-4. Stage-by-stage multivariate modeling on the large lung cancer set was carried out using multivariate logistic regression, with performance assessed by leave-one-out cross-validation, and model selection was carried out using a best subsets procedure. These analyses were carried out using R version 3.3.3. The ability of particular glycan nodes to predict cancer progression and survival was assessed via Cox proportional hazards regression models using XLSTAT Version 2012.3.01, the results of which were verified (duplicated) using SAS 9.4. Survival curves were generated and associated log-rank Mantel–Cox tests were carried out using GraphPad Prism 7.

RESULTS

Prior to initiating this study, matched collections of serum and several different types of plasma were acquired from healthy donors. Glycan nodes were analyzed in these samples to determine whether subtle differences in sample matrix (i.e., different anticoagulants and serum) impacted the analytical results. Only a few statistically significant differences between the P/S matrices were observed (Tables S2 and S3). Sodium citrate and sodium EDTA plasma samples were excluded from this study, which accounts for all of the pair-wise differences observed in Table S2; a few remaining differences (noted within the smaller sample set involving heparin plasma; Table S3), while statistically significant, were small and actually within the interassay precision range for the relevant markers.[19] A

DOI: 10.1021/acs.jproteome.7b00672
J. Proteome Res. 2018, 17, 543–558

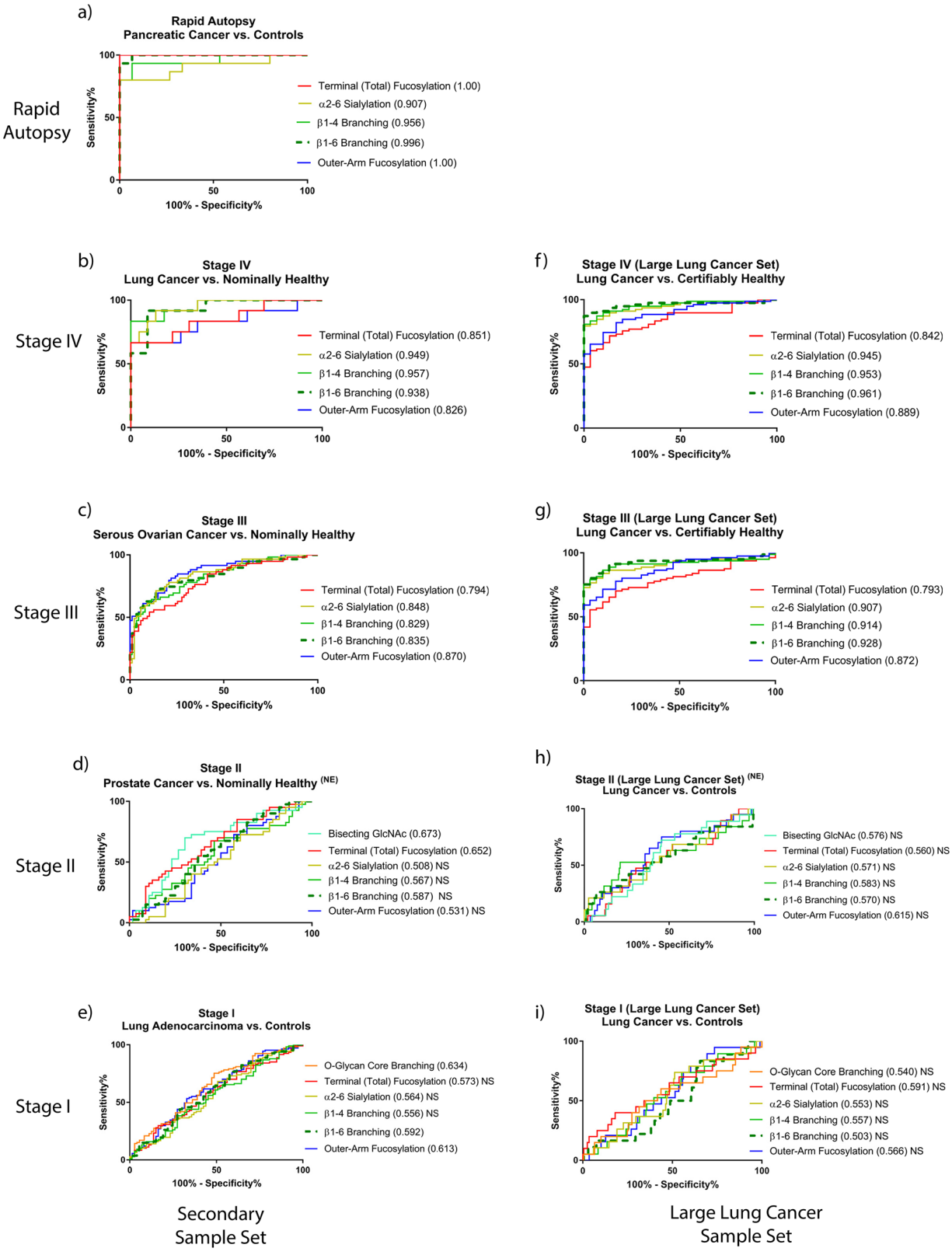

Figure 4. ROC curves depicting the stage-dependent performance of the top five-performing glycan nodes in distinguishing different types of cancer from controls or healthy individuals (panels a–e). Adjacent to panels b–e are ROC curves from the large lung cancer study for comparison (panels f–i). Clear stage dependence is evident regardless of the type of cancer involved. A comparison of each ROC curve at each stage in the large lung cancer study to the parallel ROC curve in a different type of cancer or different lung cancer sample set revealed no significant differences between ROC curves (DeLong's test; see Table S5). A superscript "NE" (panels d and h) indicates that these data sets were normalized to the sum of endogenous hexoses or HexNAcs because heavy labeled internal standards were not added during analysis of the prostate cancer sample set.

DOI: 10.1021/acs.jproteome.7b00672
J. Proteome Res. 2018, 17, 543–558

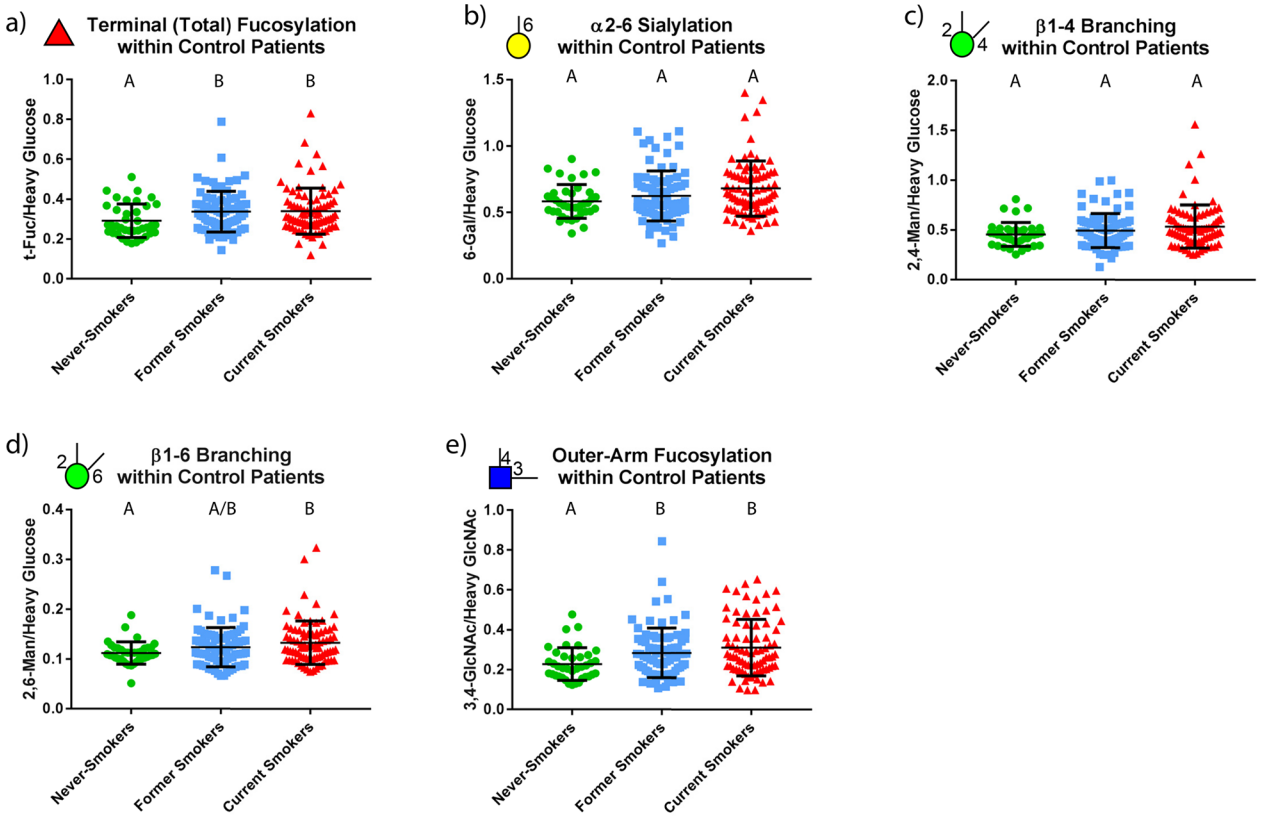

Figure 5. Univariate distributions of the top five-performing glycan nodes within the control group of the large lung cancer set, subdivided on the basis of smoking status. Letters above the data points indicate statistically significant differences between the three groups shown; any overlap in lettering between groups indicates a lack of significant difference between the groups (Kruskal–Wallis; Bonferroni-corrected p values of <0.0167 for within-group pairwise comparisons were considered statistically significant).

summary of all sample sets analyzed as part of this study is provided in Table 1.

The primary focus of this study was the large lung cancer set as it constituted the single largest set and covered all stages of cancer. In total, 19 glycan "nodes" were measured with relative abundances that were consistently greater than 1% of respective total hexoses or total *N*-acetylhexosamines (HexNAcs). As reported elsewhere, this threshold ensures quantitative precision between batches of samples.[18,19] Relative to the age-, gender-, and smoking-status-matched controls, significant changes were observed in 4 out of 19, 2 out of 19, 17 out of 19, and 17 out of 19 nodes in plasma samples taken from stage I, II, III, and IV patients, respectively (Table 2). Based on normalization to heavy, stable isotope-labeled glucose and GlcNAc internal standards, all altered glycan nodes except 4-Glc (which is mostly derived from glycolipids) were elevated in the cancer patients relative to the controls. Analogous results for data in which each hexose was normalized to the sum of endogenous hexoses and each HexNAc was normalized to the sum of endogenous HexNAcs revealed that this alternate normalization procedure is not as effective at teasing out differences between the cohorts in the large lung cancer study (Table S4).

Highly Altered Glycan Features

The five glycan nodes that were most elevated in the cancer cases relative to the at-risk controls included the following: (1) terminal fucose, which corresponds to essentially all fucose in blood plasma (nonterminal fucose is only found in notch proteins,[18,28] which, at most, would contribute only an infinitesimal fraction of the fucose found in blood plasma and, if ever detected by the approach employed here, would be observed as 3-linked fucose); (2) 6-linked galactose, which corresponds specifically to α2−6 sialylation and almost completely to the activity of the ST6GalI glycosyltransferase enzyme;[18] (3) 2,4-linked mannose, which corresponds to β1−4 branching of N-linked glycans and almost completely to the activity of the GnT-IVa enzyme;[18] (4) 2,6-linked mannose, which corresponds to β1−6 branching of N-linked glycans and to the activity of the GnT-V enzyme;[18] and (5) 3,4-linked *N*-acetylglucosamine (GlcNAc), which predominately corresponds to outer-arm fucosylation and the activity of the FucT-III, FucT-V, FucT-VI, and FucT-XI enzymes.[18] The univariate distributions of these five glycan nodes (normalized to heavy glucose or heavy GlcNAc added as an internal standard), along with receiver operating characteristic (ROC) curves that describe the potential clinical relevance of their distributions, are shown in Figure 3.

Stage and Health-Status Dependence

Table 2 and Figure 3 illustrate both the strong stage dependence of these glycan features as well as the notable contrast of their distributions in certifiably healthy individuals compared to the general middle-aged to elderly population (i.e., "controls") who are at a similar risk for cancer as individuals who actually had cancer. Similar distributions and trends were noted when the five glycan nodes were normalized to the sum of endogenous hexoses or HexNAcs, but the ROC c-statistics (areas under the curve, AUCs) tended not to be as large (Figure S1). The average age of the certifiably healthy living

DOI: 10.1021/acs.jproteome.7b00672
J. Proteome Res. 2018, 17, 543−558

kidney donor population was 47, and that of both the controls and lung cancer cases in this set of samples was 61 (Table S1). However, after pooling data from the certifiably healthy donors, controls and lung cancer cases and correcting for multiple comparisons, no statistically significant correlations with age were observed for any of these glycan nodes. (Before correcting for multiple comparisons, terminal (total) fucose appeared slightly correlated with age (Pearson correlation of R^2 = 0.013 and p = 0.021), but this result cannot be considered statistically significant after considering the fact that multiple comparisons were made.) Likewise, no statistically significant correlations of glycan nodes with age were observed when these groups of patients were evaluated individually.

In general, the five glycan nodes increased together as the stage of cancer advanced (Figure 4). Moreover, the behavior of these nodes was independent of the organ of tumor origin, at least when comparing lung cancer with pancreatic, ovarian, and prostate cancers. This was quantitatively evident when the ROC curves in panels c and d of the left column of Figure 4 were statistically compared with ROC curves from their respective lung cancer stages shown in the right column (Table S5). At stage IV, both outer-arm fucosylation and terminal (total) fucosylation lag a bit behind α2−6 sialylation, β1−4 branching, and β1−6 branching, but fucosylation-related nodes caught up and even surpassed these other glycan features once cancer had fully run its course (Figure 4a). When stage was held constant, no glycan nodes were found to be significantly different between adenocarcinoma, squamous cell carcinoma and small cell carcinoma, the three different histological subtypes observed in the large lung cancer study (Table S1). However, terminal (total) fucosylation, β1−6 branching, and outer-arm fucosylation were altered within the control cohort on the basis of smoking status (grouped as never-smokers, former smokers, or current smokers; Figure 5).

Orthogonality of Glycan Features

To evaluate the orthogonality of all 19 glycan nodes included in this study (Table 2), multivariate logistic regression models were created for the large lung cancer set on a stage-by-stage basis (Figure 6). Results of modeling are shown as ROC curves, where the model-derived predicted probability of disease for the sample was used as the discriminatory variable. In summary, the fully cross-validated forms of these multivariate logistic regression models do not distinguish lung cancer cases from controls any better than individual glycan nodes (cf. Figure 4f−i). This indicates a general lack of orthogonality or independence between the glycan features observed in this study.

Comparison to Liver Fibrosis

The vast majority of glycoproteins found in blood P/S are derived from either liver glycoproteins or immunoglobulins (IgG molecules) secreted by the immune system.[29,30] In terms of raw abundance, which is in the range of tens of milligrams per milliliter, the relative contribution of P/S glycoproteins provided by the liver and by the immune system is approximately 50% each.[30] Essentially all nonprotein targeting serum glycomics approaches, including the one employed in this study, detect changes in these abundant P/S glycans and not novel glycans secreted or sloughed-off by cancer cells. This concept has been acknowledged elsewhere.[31] Nevertheless, P/S glycans are notoriously known for being altered in cancer.[1−4,32] However, they are also known to be altered in inflammatory conditions in the absence of cancer.[33−35] As an initial attempt

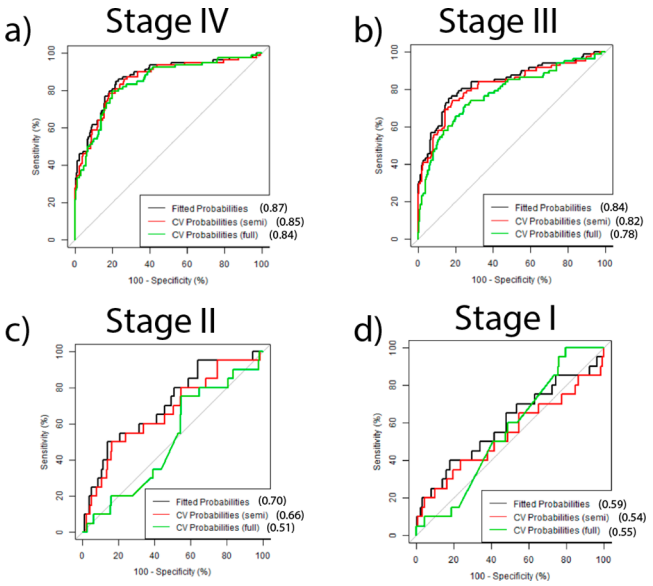

Figure 6. Multivariate logistic regression models for stage I−IV lung cancer patients from the large lung cancer data set. Fully validated multivariate combinations of glycan nodes did not produce significantly better ROC curves in stage IV, III, II, or I lung cancer patients (panels a−d, respectively) compared to the best-performing individual glycan node in the control specimens (DeLong test). A total of three separate curves are shown on each plot, corresponding to predicted probabilities derived from a multivariate logistic regression model (1) refitted at each iteration of cross-validation (referred to as "CV Probabilities (full)"); (2) fitted once on the complete data set, fixing the predictors but allowing parameter estimates to change at each iteration of cross-validation (referred to as "CV Probabilities (semi)"); and (3) fitted once on the complete data set and taking the model-derived probability without use of cross-validation (referred to as "Fitted Probabilities").

to begin to parse out the behavior of the five glycan nodes that were most elevated in the large lung cancer set, they were analyzed in a set of serum samples from liver fibrosis patients (Figure 7). Statistical analysis (Kruskal−Wallis) indicated that there were no significant differences in any of the glycan nodes shown across all stages of liver fibrosis. This may have been due to limited statistical power. Notably, however, fucosylation-related markers exhibited a tendency to be elevated in stage III−IV liver fibrosis.

Prediction of Progression and All-Cause Mortality

The five glycan nodes that were most elevated in the large lung cancer set were evaluated for their ability to predict both progression and all-cause mortality in a Cox proportional hazards regression model. After adjustment for age, gender, smoking status, and cancer stage, only 6-linked galactose, which corresponds to α2−6 sialylation, predicted both progression and all-cause mortality with p-values of <0.01 when the glycan nodes were modeled as continuous variables. All four other top-performing glycan nodes were able to predict survival (p < 0.05), but only β1−4 branching and β1−6 branching were also able to predict progression (p < 0.05). Because relative rather than absolute quantification was employed, glycan node units lack readily interpretable meaning. As such, measurements of α2−6 sialylation were broken into quartiles, and the Cox proportional hazards analysis repeated. After adjustment for age, gender, smoking status, and cancer stage, the top α2−6 sialylation quartile predicted progression with a hazard ratio of

DOI: 10.1021/acs.jproteome.7b00672
J. Proteome Res. 2018, 17, 543−558

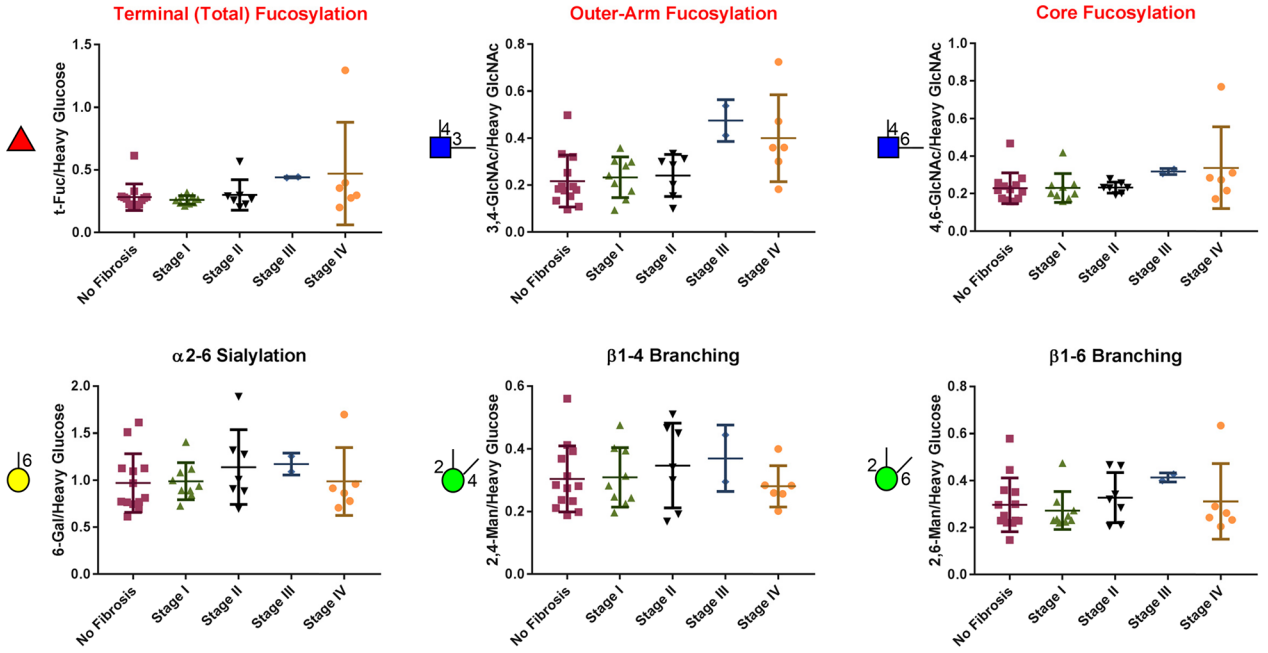

Figure 7. Univariate distributions of fucosylation-related glycan nodes, α2−6 sialylation, β1−4 branching, and β1−6 branching in stage 0 through stage IV liver fibrosis. No statistically significant differences were observed for any pairwise comparisons within a single glycan node (Kruskal−Wallis).

2.45 relative to all other quartiles combined (lower bound at 95% CL = 1.54; upper bound at 95% CL = 3.90; $p = 1.5 \times 10^{-4}$). Likewise, after the same adjustments, the top α2−6 sialylation quartile predicted all-cause mortality with a hazard ratio of 1.52 relative to all other quartiles combined (lower bound at 95% CL = 1.02; upper bound at 95% CL = 2.23; $p = 0.042$). Progression and survival curves illustrate the differences in the rates of occurrence of these events for the top α2−6 sialylation quartile versus all other quartiles (Figure 8). Progression and survival curves for stage III patients alone illustrate that the separation of progression by α2−6 sialylation and the separation of survival by α2−6 sialylation is not simply driven by stage (Figure 8c,d). α2−6 sialylation was not elevated or able to predict progression or survival in the stage I lung adenocarcinoma set.

DISCUSSION

The five glycan features that were most elevated relative to healthy individuals and at-risk controls were terminal (total) fucosylation, α2−6 sialylation, β1−4 branching, β1−6 branching, and outer-arm fucosylation (Table 2 and Figures 3 and 4). A pair of phenomena stood out most with regard to their distributions among the cohorts of the large lung cancer study: First, there was a striking stage dependence of all five glycan features that was independent of the tumor organ of origin (Table 2, Figures 3 and 4, and Table S5). In part, statistical significance at earlier stages may not have been achieved due to the relatively low number of samples measured from patients at stages I−II ($n \approx 20$ per stage). Statistically significant elevation of core-branched O-glycans (i.e., 3,6-linked GalNAc) over age-, gender-, and smoking-status-matched controls was observed in stage I lung adenocarcinoma from this separate, larger set of samples (Figure 4). However, it was clear from the ROC curve (Figure 4e) that this glycan node cannot serve as a useful early stage diagnostic biomarker.

A second notable feature apparent in the large lung cancer set was the statistically significant difference between certifiably healthy living kidney donors and risk-matched controls for α2−6 sialylation, β1−4 branching, and β1−6 branching, with controls always increased toward the direction of cancer (Table 2 and Figure 3). These differences between certifiably healthy individuals and patients with an elevated risk of cancer underscore the high risk of false discovery when nominally healthy sample donors rather than well-characterized, clinically relevant controls are employed during biomarker development. The notable differences between healthy individuals and at-risk controls also support the idea that the biological landscape within plasma and serum may undergo "grooming", "conditioning", or premetastatic "niche" formation prior to cancer taking hold within the body.[36−40] Given that inflammation is closely tied to the development of cancer[41,42] and that at least some glycans and glycan features are known to be altered in inflammatory conditions in the absence of cancer,[33−35] precancerous inflammation may be responsible for the elevation of many of the glycan features observed in the at-risk controls relative to the certifiably healthy living kidney donors, suggesting that the goal of preventing such a precancerous state may be as important as preventing the transition from an at-risk state to stage I cancer. With this in mind, it is interesting to note that about 62% of the age-qualified U.S. population would be excluded as living kidney donors due to preventable health conditions.[43]

A few studies have been published that are closely related to the one reported here but in which intact glycans were analyzed.[31,44,45] While not in conflict with any of these studies, our most prominent findings of increased terminal (total) fucosylation, α2−6 sialylation, β1−4 branching, β1−6 branching, and outer-arm fucosylation in stage III−IV lung cancer are most closely aligned with the major changes reported by Vasseur et al.[31] for intact glycans in lung cancer. They reported significant increases in fucosylated tri- and tetra-antennary

DOI: 10.1021/acs.jproteome.7b00672
J. Proteome Res. 2018, 17, 543−558

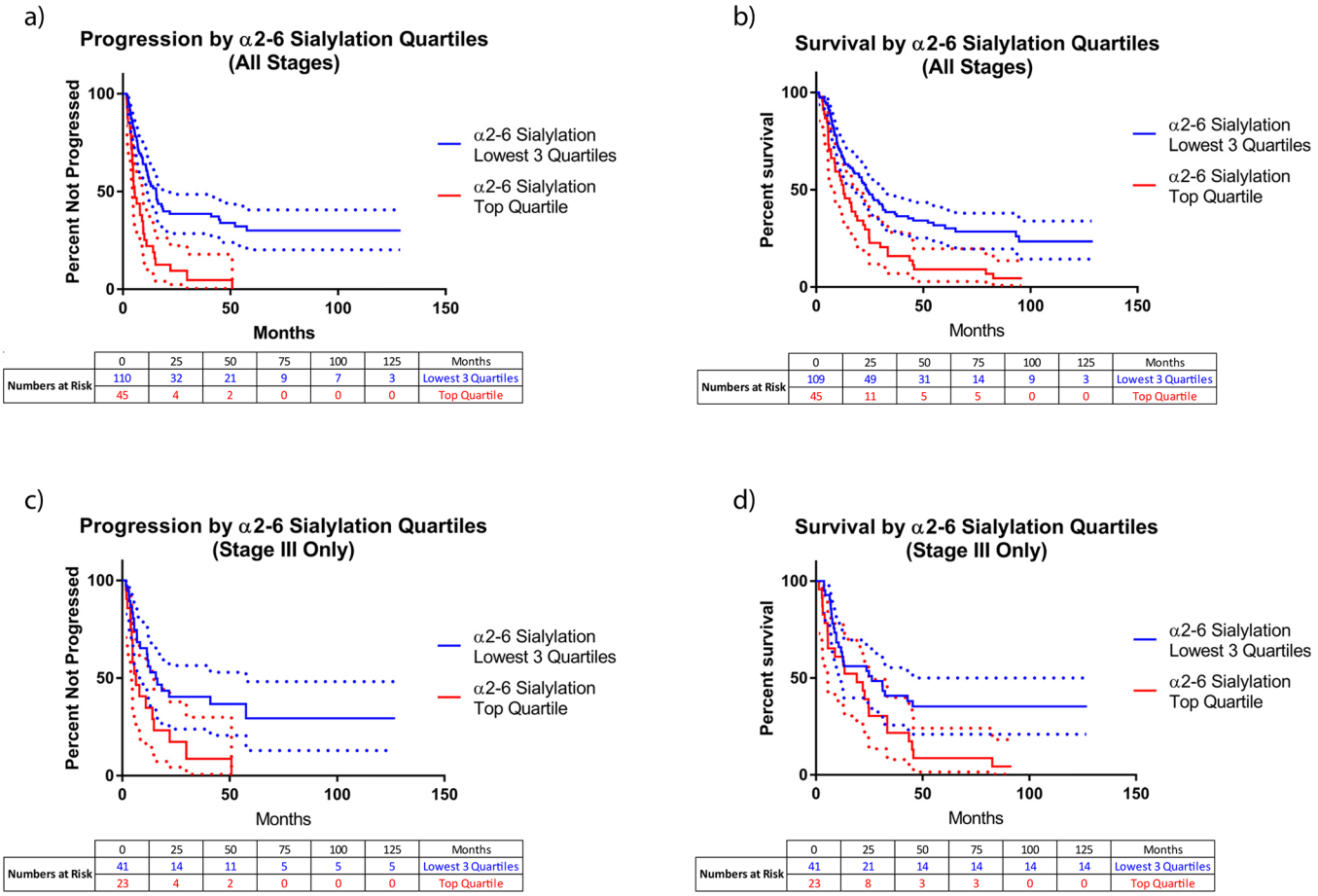

Figure 8. Large lung cancer data set progression (i.e., progression-free survival; panels a and c) and survival (all-cause mortality; panels b and d) curves for the top $\alpha 2-6$ sialylation quartile compared to all other quartiles combined. Panels a and b combine data from all stages; panels c and d present data from stage III only, illustrating that curve separation based on $\alpha 2-6$ sialylation is not simply driven by stage. Dotted lines represent 95% confidence intervals, colored according to their respective curves. Within each plot, progression curves were significantly different from one another (log-rank Mantel-Cox test; $p < 0.01$) as were the survival curves (log-rank Mantel-Cox test; $p < 0.05$). For the progression data (all stages; panel a), the median duration of follow-up for those that progressed, until progression, was 6.9 months (17.1 months median total follow-up time); for those that did not progress, the median duration of follow-up was 22.7 months. Results from Cox proportional hazards models are described in the Results section.

structures, outer-arm fucosylated structures, and $\alpha 2-6$ sialylated structures. Moreover, they reported that all of these features were elevated in control-group former smokers relative to control group nonsmokers. We found increases in terminal (total) fucosylation, $\beta 1-6$ branching, and outer-arm fucosylation in current smokers relative to people who never smoked but only increases in terminal (total) fucosylation and outer-arm fucosylation in former smokers relative to people who had never smoked (Figure 5). Notably, the method employed for the analysis of intact glycans by Vasseur et al. is one of just a few approaches that are capable of distinguishing 6-linked from 3-linked sialic acid.[46−48]

Multivariate logistic regression models were not able to outperform individual glycan nodes (cf. Figures 4f−i and 6) with regard to distinguishing cancer at stages I−IV from controls. This indicates a general lack of biological orthogonality among the abnormal glycan features observed, suggesting that they likely have a singular (or small set of closely related) upstream causes. The concentration of glycoproteins in P/S is in the range of tens of milligrams per milliliter. As such, the observations of significant changes in P/S glycans observed here cannot be due to glycoproteins shed directly from cancer cells; almost certainly, they are derived from alterations to one or both of the two major sources of P/S glycoproteins, namely liver glycoproteins or immunoglobulins (IgG molecules) secreted by the immune system.[29,30] Such alterations are thought to be mediated by cytokines secreted from the tumor microenvironment and exist as part of an acute-phase inflammatory response.[31,49−53]

However, this is not to imply that liver glycoprotein and immunoglobulin glycan alterations are unimportant or lack a cancer-relevant pathological effect. Several cancer up-regulated glycoforms that cancer cells have in common with glycans that are induced on acute-phase liver proteins and/or IgG molecules in the presence of cancer have been found to mediate specific immune-modulating effects, some of which overtly favor cancer progression:

Galectins are a family of lectins that bind β-galactoside sugars within glycans and are known to modulate a variety of immunological processes involved in cancer.[39,54,55] Malignant T-cells in mycosis fungoides/Sezary syndrome have been found to resist galectin-1 mediated apoptosis because they both lack the CD7 receptors that carry the oligosaccharides recognized by galectin-1 and because they express sialylated core 1 O-glycans that promote galectin-1 resistance.[56] Poly-*N*-acetyllactosamine-modified core 2 O-glycans bind to galectin-3,

DOI: 10.1021/acs.jproteome.7b00672
J. Proteome Res. 2018, 17, 543−558

reducing the affinity of tumor major histocompatibility complex (MHC) class I-related chain A (MICA) for the activating NKG2D receptor on natural killer (NK) cells, preventing the tumor-cell killing of core 2 O-glycan expressing cancer cells.[57−60] Similarly, modification of MUC1 by poly-*N*-acetyllactosamine and subsequent binding by galectin-3 interferes with TRAIL-mediated killing of DR4-expressing cancer cells by NK cells.[60−62] However, perhaps the best-known example is the ability of excessive tumor cell surface sialylation to stimulate the inhibitory Siglec-7 receptor on NK cells, preventing their activation.[60,63−65]

In light of these discoveries, the fact that α2−6 sialylation of abundant plasma and serum proteins is both associated with metastasis and poor prognosis[66,67] and, in our study, was not only elevated in lung cancer but also predicted progression and all-cause mortality in the large lung cancer set may shed additional light on a means by which cancer potentially manipulates the immune system to groom the physiological landscape and carve out a metastatic niche. Rather than directly interacting (cell-to-cell) with NK cells, tumor cells may simply be able to send out cytokine signals that are picked up by the liver and the immune system that alter the way that these nominally healthy tissues glycosylate their secreted proteins. This could, for example, facilitate a large-scale amplification of sialylated glycans that are able to continually activate Siglec-7 receptors on NK cells, preventing them from killing tumor cells and allowing them to metastasize. The possibility that cancer cells may induce the abnormal glycosylation of the highly abundant liver glycoproteins and IgG molecules found in P/S as a shielding mechanism against innate immune detection during metastasis attempts has received very little attention but may be worth investigating. Though speculative, this strategy could even potentially be deployed in cases in which cancer cells deplete themselves of a glycan feature required for immune-cell recognition, such as the fucosylation recognized by the TRAIL-mediate killing mechanism of NK cells,[68] but induce it on abundant P/S proteins, serving to "swamp out" the recognition mechanism of innate immune surveillance.

The ability of α2−6 sialylation to predict lung cancer progression and survival is not unique among P/S glycans. Indeed, all five top-performing glycan nodes in the present study were able to predict progression and survival to a more-limited extent than α2−6 sialylation. The prognostic capacity of β1−4 and β1−6 branching, however, may, at least in part, be due to the fact that these glycan features simply create greater opportunity for sialylation. Beyond this study, others have found that the sialyl Lewis X epitope (which displays α2−3 sialylation rather than α2−6 sialylation) predicts progression and survival in both small-cell[69] and non-small-cell lung cancer.[70−72] Like the prognostic Veristrat markers,[73−75] which are serum amyloid A proteoforms,[76] elevated α2−6 sialylation in lung cancer may largely be due to an inflammatory response by the liver. However, if, as described above, sialylation-based cloaking of tumor cells from the immune system plays an important role in the metastatic process, α2−6 sialylation may turn out to play a causative, mechanistic role in lung cancer progression.

CONCLUSIONS

A molecularly bottom-up approach to plasma and serum (P/S) glycomics based on glycan linkage analysis that captures unique glycan features such as α2−6 sialylation, β1−6 branching, and core fucosylation as single analytical signals was employed to evaluate the behavior of P/S glycans in all stages of lung cancer and across various stages of prostate, ovarian and pancreatic cancers. Elevation of terminal (total) fucosylation, α2−6 sialylation, β1−4 branching, β1−6 branching, and outer-arm fucosylation markers were most pronounced in lung cancer in a stage-dependent manner, but these changes were found to be independent of the tumor tissue-of-origin. Using a Cox proportional hazards regression model, the marker for α2−6 sialylation was found to predict both progression and all-cause mortality in lung cancer patients after adjusting for age, gender, smoking status, and stage at which the sample was taken. Interestingly, certifiably healthy P/S donors had markedly lower levels of α2−6 sialylation, β1−4 branching, and β1−6 branching relative to cancer risk-matched controls. While early detection is ideal, the information provided by this and related studies[31,33−35,41,42,49−53] suggests that precancerous inflammation may be responsible for the elevation of many of the glycan features observed in the at-risk controls relative to the certifiably healthy donors, implying that the goal of preventing such a precancerous state may be as important as preventing the transition from an at-risk state to stage I cancer.

ASSOCIATED CONTENT

Supporting Information

The Supporting Information is available free of charge on the ACS Publications website at DOI: 10.1021/acs.jproteome.7b00672.

Tables showing basic clinical characteristics and n-values, the impact of plasma and serum matrices on glycan node measurements, a comparison of sodium heparin plasma to potassium EDTA plasma and serum matrices, statistically significant differences between cohorts within the large lung cancer study, and a stage-by-stage comparison of the top-performing glycan nodes. Figures showing univariate distributions and associated ROC curves for the top five-performing glycan nodes in the large lung cancer set when data were normalized to the sum of endogenous hexoses or HexNAcs. An appendix showing the inclusion and exclusion criteria for certifiably healthy living kidney donors. (PDF)

Ferdosi et al. All Data.xlsm − Raw and normalized chromatographic peak areas for all clinical samples in this study

AUTHOR INFORMATION

Corresponding Author

*E-mail: chad.borges@asu.edu. Phone: 480-727-9928.

ORCID

Shadi Ferdosi: 0000-0003-2933-8809

Chad R. Borges: 0000-0002-8122-3438

Present Address

⊙Gilead Sciences, Inc. 4049 Avenida de la Plata Oceanside, CA 92056, United States.

Notes

The authors declare no competing financial interest.

ACKNOWLEDGMENTS

We are grateful to Michael A. Hollingsworth of the University of Nebraska Medical Center for sharing the rapid autopsy pancreatic cancer sample set. The research reported in this

DOI: 10.1021/acs.jproteome.7b00672
J. Proteome Res. 2018, 17, 543−558

publication was supported in part by the Flinn Foundation (grant no. 1977 to C.B.), the Gerstner Family Career Development Award, the Gloria A. and Thomas J. Dutson Jr. Kidney Research Endowment (to T.H.), the University of Texas MD Anderson Cancer Center and The Center for Translational and Public Health Genomics (to X.W.), and the National Cancer Institute of the National Institutes of Health under award no. R33 CA191110 (to C.B.), and award nos. P50 CA070907 and R01 CA176568 (to X.W.). The content is solely the responsibility of the authors and does not necessarily represent the official views of the Flinn Foundation or the National Institutes of Health.

REFERENCES

(1) Varki, A.; Kannagi, R.; Toole, B., Glycosylation Changes in Cancer. In *Essentials of Glycobiology*, 2nd ed.; Varki, A.; Cummings, R. D.; Esko, J. D.; Freeze, H. H.; Stanley, P.; Bertozzi, C. R.; Hart, G. W.; Etzler, M. E., Eds; Cold Spring Harbor Laboratory Press: Cold Spring Harbor, NY, 2009; pp 617−632.

(2) Kailemia, M. J.; Park, D.; Lebrilla, C. B. Glycans and glycoproteins as specific biomarkers for cancer. *Anal. Bioanal. Chem.* **2017**, *409* (2), 395−410.

(3) Lauc, G.; Pezer, M.; Rudan, I.; Campbell, H. Mechanisms of disease: The human N-glycome. *Biochim. Biophys. Acta, Gen. Subj.* **2016**, *1860* (8), 1574−82.

(4) Almeida, A.; Kolarich, D. The promise of protein glycosylation for personalised medicine. *Biochim. Biophys. Acta, Gen. Subj.* **2016**, *1860* (8), 1583−95.

(5) An, H. J.; Miyamoto, S.; Lancaster, K. S.; Kirmiz, C.; Li, B.; Lam, K. S.; Leiserowitz, G. S.; Lebrilla, C. B. Profiling of glycans in serum for the discovery of potential biomarkers for ovarian cancer. *J. Proteome Res.* **2006**, *5* (7), 1626−35.

(6) Ruhaak, L. R.; Miyamoto, S.; Lebrilla, C. B. Developments in the identification of glycan biomarkers for the detection of cancer. *Mol. Cell. Proteomics* **2013**, *12* (4), 846−55.

(7) Hajba, L.; Csanky, E.; Guttman, A. Liquid phase separation methods for N-glycosylation analysis of glycoproteins of biomedical and biopharmaceutical interest. A critical review. *Anal. Chim. Acta* **2016**, *943*, 8−16.

(8) Frost, D. C.; Li, L. Recent advances in mass spectrometry-based glycoproteomics. *Adv. Protein Chem. Struct. Biol.* **2014**, *95*, 71−123.

(9) Mechref, Y.; Hu, Y.; Garcia, A.; Hussein, A. Identifying cancer biomarkers by mass spectrometry-based glycomics. *Electrophoresis* **2012**, *33* (12), 1755−67.

(10) Hennig, R.; Cajic, S.; Borowiak, M.; Hoffmann, M.; Kottler, R.; Reichl, U.; Rapp, E. Towards personalized diagnostics via longitudinal study of the human plasma N-glycome. *Biochim. Biophys. Acta, Gen. Subj.* **2016**, *1860* (8), 1728−38.

(11) Verhelst, X.; Vanderschaeghe, D.; Castera, L.; Raes, T.; Geerts, A.; Francoz, C.; Colman, R.; Durand, F.; Callewaert, N.; Van Vlierberghe, H. A Glycomics-Based Test Predicts the Development of Hepatocellular Carcinoma in Cirrhosis. *Clin. Cancer Res.* **2017**, *23* (11), 2750−2758.

(12) Saldova, R.; Shehni, A. A.; Haakensen, V. D.; Steinfeld, I.; Hilliard, M.; Kifer, I.; Helland, A.; Yakhini, Z.; Borresen-Dale, A. L.; Rudd, P. M. Association of N-Glycosylation with Breast Carcinoma and Systemic Features Using High-Resolution Quantitative UPLC. *J. Proteome Res.* **2014**, *13* (5), 2314−2327.

(13) Hua, S.; An, H. J.; Ozcan, S.; Ro, G. S.; Soares, S.; DeVere-White, R.; Lebrilla, C. B. Comprehensive native glycan profiling with isomer separation and quantitation for the discovery of cancer biomarkers. *Analyst* **2011**, *136* (18), 3663−71.

(14) Hua, S.; Jeong, H. N.; Dimapasoc, L. M.; Kang, I.; Han, C.; Choi, J. S.; Lebrilla, C. B.; An, H. J. Isomer-specific LC/MS and LC/MS/MS profiling of the mouse serum N-glycome revealing a number of novel sialylated N-glycans. *Anal. Chem.* **2013**, *85* (9), 4636−43.

(15) Klasic, M.; Kristic, J.; Korac, P.; Horvat, T.; Markulin, D.; Vojta, A.; Reiding, K. R.; Wuhrer, M.; Lauc, G.; Zoldos, V. DNA hypomethylation upregulates expression of the MGAT3 gene in HepG2 cells and leads to changes in N-glycosylation of secreted glycoproteins. *Sci. Rep.* **2016**, *6*, 24363.

(16) Kolarich, D.; Lepenies, B.; Seeberger, P. H. Glycomics, glycoproteomics and the immune system. *Curr. Opin. Chem. Biol.* **2012**, *16* (1−2), 214−20.

(17) Sethi, M. K.; Fanayan, S. Mass Spectrometry-Based N-Glycomics of Colorectal Cancer. *Int. J. Mol. Sci.* **2015**, *16* (12), 29278−304.

(18) Borges, C. R.; Rehder, D. S.; Boffetta, P. Multiplexed surrogate analysis of glycotransferase activity in whole biospecimens. *Anal. Chem.* **2013**, *85* (5), 2927−36.

(19) Zaare, S.; Aguilar, J. S.; Hu, Y.; Ferdosi, S.; Borges, C. R. Glycan Node Analysis: A Bottom-up Approach to Glycomics. *J. Visualized Exp.* **2016**, *111*, No. e53961, DOI: 10.3791/53961.

(20) Hu, Y.; Borges, C. R. A spin column-free approach to sodium hydroxide-based glycan permethylation. *Analyst* **2017**, *142* (15), 2748−2759.

(21) Ho, T. H.; Nateras, R. N.; Yan, H.; Park, J. G.; Jensen, S.; Borges, C.; Lee, J. H.; Champion, M. D.; Tibes, R.; Bryce, A. H.; Carballido, E. M.; Todd, M. A.; Joseph, R. W.; Wong, W. W.; Parker, A. S.; Stanton, M. L.; Castle, E. P. A Multidisciplinary Biospecimen Bank of Renal Cell Carcinomas Compatible with Discovery Platforms at Mayo Clinic, Scottsdale, Arizona. *PLoS One* **2015**, *10* (7), e0132831.

(22) Grizzle, W. E.; Gunter, E. W.; Sexton, K. C.; Bell, W. C. Quality management of biorepositories. *Biopreserv. Biobanking* **2015**, *13* (3), 183−94.

(23) Katchman, B. A.; Chowell, D.; Wallstrom, G.; Vitonis, A. F.; LaBaer, J.; Cramer, D. W.; Anderson, K. S. Autoantibody biomarkers for the detection of serous ovarian cancer. *Gynecol. Oncol.* **2017**, *146* (1), 129−136.

(24) Anderson, K. S.; Cramer, D. W.; Sibani, S.; Wallstrom, G.; Wong, J.; Park, J.; Qiu, J.; Vitonis, A.; LaBaer, J. Autoantibody signature for the serologic detection of ovarian cancer. *J. Proteome Res.* **2015**, *14* (1), 578−86.

(25) Katchman, B. A.; Barderas, R.; Alam, R.; Chowell, D.; Field, M. S.; Esserman, L. J.; Wallstrom, G.; LaBaer, J.; Cramer, D. W.; Hollingsworth, M. A.; Anderson, K. S. Proteomic mapping of p53 immunogenicity in pancreatic, ovarian, and breast cancers. *Proteomics: Clin. Appl.* **2016**, *10* (7), 720−31.

(26) Murphy, B. M.; Swarts, S.; Mueller, B. M.; van der Geer, P.; Manning, M. C.; Fitchmun, M. I. Protein instability following transport or storage on dry ice. *Nat. Methods* **2013**, *10* (4), 278−9.

(27) Borges, C. R.; Rehder, D. S.; Jensen, S.; Schaab, M. R.; Sherma, N. D.; Yassine, H.; Nikolova, B.; Breburda, C. Elevated Plasma Albumin and Apolipoprotein A-I Oxidation under Suboptimal Specimen Storage Conditions. *Mol. Cell. Proteomics* **2014**, *13* (7), 1890−9.

(28) Moloney, D. J.; Shair, L. H.; Lu, F. M.; Xia, J.; Locke, R.; Matta, K. L.; Haltiwanger, R. S. Mammalian Notch1 is modified with two unusual forms of O-linked glycosylation found on epidermal growth factor-like modules. *J. Biol. Chem.* **2000**, *275* (13), 9604−9611.

(29) Anderson, N. L.; Anderson, N. G. The human plasma proteome: history, character, and diagnostic prospects. *Mol. Cell. Proteomics* **2002**, *1* (11), 845−67.

(30) Baker, E. S.; Liu, T.; Petyuk, V. A.; Burnum-Johnson, K. E.; Ibrahim, Y. M.; Anderson, G. A.; Smith, R. D. Mass spectrometry for translational proteomics: progress and clinical implications. *Genome Med.* **2012**, *4* (8), 63.

(31) Vasseur, J. A.; Goetz, J. A.; Alley, W. R., Jr.; Novotny, M. V. Smoking and lung cancer-induced changes in N-glycosylation of blood serum proteins. *Glycobiology* **2012**, *22* (12), 1684−708.

(32) Miura, Y.; Endo, T. Glycomics and glycoproteomics focused on aging and age-related diseases - Glycans as a potential biomarker for physiological alterations. *Biochim. Biophys. Acta, Gen. Subj.* **2016**, *1860* (8), 1608−1614.

(33) Miyahara, K.; Nouso, K.; Saito, S.; Hiraoka, S.; Harada, K.; Takahashi, S.; Morimoto, Y.; Kobayashi, S.; Ikeda, F.; Miyake, Y.; Shiraha, H.; Takaki, A.; Okada, H.; Amano, M.; Hirose, K.; Nishimura,

DOI: 10.1021/acs.jproteome.7b00672
J. Proteome Res. 2018, 17, 543−558

S.; Yamamoto, K. Serum glycan markers for evaluation of disease activity and prediction of clinical course in patients with ulcerative colitis. *PLoS One* **2013**, *8* (10), e74861.
(34) Vanderschaeghe, D.; Laroy, W.; Sablon, E.; Halfon, P.; Van Hecke, A.; Delanghe, J.; Callewaert, N. GlycoFibroTest Is a Highly Performant Liver Fibrosis Biomarker Derived from DNA Sequencer-based Serum Protein Glycomics. *Mol. Cell. Proteomics* **2009**, *8* (5), 986−994.
(35) Callewaert, N.; Van Vlierberghe, H.; Van Hecke, A.; Laroy, W.; Delanghe, J.; Contreras, R. Noninvasive diagnosis of liver cirrhosis using DNA sequencer-based total serum protein glycomics. *Nat. Med.* **2004**, *10* (4), 429−434.
(36) Wysoczynski, M.; Ratajczak, M. Z. Lung cancer secreted microvesicles: underappreciated modulators of microenvironment in expanding tumors. *Int. J. Cancer* **2009**, *125* (7), 1595−603.
(37) Martins, V. R.; Dias, M. S.; Hainaut, P. Tumor-cell-derived microvesicles as carriers of molecular information in cancer. *Curr. Opin. Oncol.* **2013**, *25* (1), 66−75.
(38) Simona, F.; Laura, S.; Simona, T.; Riccardo, A. Contribution of proteomics to understanding the role of tumor-derived exosomes in cancer progression: state of the art and new perspectives. *Proteomics* **2013**, *13* (10−11), 1581−1594.
(39) Rabinovich, G. A.; Conejo-Garcia, J. R. Shaping the Immune Landscape in Cancer by Galectin-Driven Regulatory Pathways. *J. Mol. Biol.* **2016**, *428* (16), 3266−81.
(40) Sethi, M. K.; Hancock, W. S.; Fanayan, S. Identifying N-Glycan Biomarkers in Colorectal Cancer by Mass Spectrometry. *Acc. Chem. Res.* **2016**, *49* (10), 2099−2106.
(41) Hanahan, D.; Weinberg, R. A. Hallmarks of cancer: the next generation. *Cell* **2011**, *144* (5), 646−74.
(42) Wang, D.; DuBois, R. N. Immunosuppression associated with chronic inflammation in the tumor microenvironment. *Carcinogenesis* **2015**, *36* (10), 1085−93.
(43) Bleyer, A. J.; Reeves-Daniel, A. M. *A Population-Based Study of the U.S. Population Shows the Majority of Persons Cannot Donate due to Preventable Diseases and Socio-Economic Conditions*; Journal of the American Society of Nephrology: Philadelphia, PA, 2014; p 67A.
(44) Arnold, J. N.; Saldova, R.; Galligan, M. C.; Murphy, T. B.; Mimura-Kimura, Y.; Telford, J. E.; Godwin, A. K.; Rudd, P. M. Novel glycan biomarkers for the detection of lung cancer. *J. Proteome Res.* **2011**, *10* (4), 1755−64.
(45) Ruhaak, L. R.; Stroble, C.; Dai, J. L.; Barnett, M.; Taguchi, A.; Goodman, G. E.; Miyamoto, S.; Gandara, D.; Feng, Z. D.; Lebrilla, C. B.; Hanash, S. Serum Glycans as Risk Markers for Non-Small Cell Lung Cancer. *Cancer Prev. Res.* **2016**, *9* (4), 317−323.
(46) Alley, W. R., Jr.; Novotny, M. V. Glycomic analysis of sialic acid linkages in glycans derived from blood serum glycoproteins. *J. Proteome Res.* **2010**, *9* (6), 3062−72.
(47) Reiding, K. R.; Blank, D.; Kuijper, D. M.; Deelder, A. M.; Wuhrer, M. High-throughput profiling of protein N-glycosylation by MALDI-TOF-MS employing linkage-specific sialic acid esterification. *Anal. Chem.* **2014**, *86* (12), 5784−93.
(48) Holst, S.; Heijs, B.; de Haan, N.; van Zeijl, R. J.; Briaire-de Bruijn, I. H.; van Pelt, G. W.; Mehta, A. S.; Angel, P. M.; Mesker, W. E.; Tollenaar, R. A.; Drake, R. R.; Bovee, J. V.; McDonnell, L. A.; Wuhrer, M. Linkage-Specific in Situ Sialic Acid Derivatization for N-Glycan Mass Spectrometry Imaging of Formalin-Fixed Paraffin-Embedded Tissues. *Anal. Chem.* **2016**, *88* (11), 5904−13.
(49) Gryska, K.; Slupianek, A.; Laciak, M.; Gorny, A.; Mackiewicz, K.; Baumann, H.; Mackiewicz, A. Inflammatory cytokines controlling branching of N-heteroglycans of acute phase protein. *Adv. Exp. Med. Biol.* **1995**, *376*, 239−45.
(50) Narisada, M.; Kawamoto, S.; Kuwamoto, K.; Moriwaki, K.; Nakagawa, T.; Matsumoto, H.; Asahi, M.; Koyama, N.; Miyoshi, E. Identification of an inducible factor secreted by pancreatic cancer cell lines that stimulates the production of fucosylated haptoglobin in hepatoma cells. *Biochem. Biophys. Res. Commun.* **2008**, *377* (3), 792−796.
(51) Arnold, J. N.; Saldova, R.; Hamid, U. M.; Rudd, P. M. Evaluation of the serum N-linked glycome for the diagnosis of cancer and chronic inflammation. *Proteomics* **2008**, *8* (16), 3284−93.
(52) Saldova, R.; Wormald, M. R.; Dwek, R. A.; Rudd, P. M. Glycosylation changes on serum glycoproteins in ovarian cancer may contribute to disease pathogenesis. *Dis. Markers* **2008**, *25* (4−5), 219−232.
(53) Sarrats, A.; Saldova, R.; Pla, E.; Fort, E.; Harvey, D. J.; Struwe, W. B.; de Llorens, R.; Rudd, P. M.; Peracaula, R. Glycosylation of liver acute-phase proteins in pancreatic cancer and chronic pancreatitis. *Proteomics: Clin. Appl.* **2010**, *4* (4), 432−48.
(54) Cagnoni, A. J.; Perez Saez, J. M.; Rabinovich, G. A.; Marino, K. V. Turning-Off Signaling by Siglecs, Selectins, and Galectins: Chemical Inhibition of Glycan-Dependent Interactions in Cancer. *Front. Oncol.* **2016**, *6*, 109.
(55) Mendez-Huergo, S. P.; Blidner, A. G.; Rabinovich, G. A. Galectins: emerging regulatory checkpoints linking tumor immunity and angiogenesis. *Curr. Opin. Immunol.* **2017**, *45*, 8−15.
(56) Roberts, A. A.; Amano, M.; Felten, C.; Galvan, M.; Sulur, G.; Pinter-Brown, L.; Dobbeling, U.; Burg, G.; Said, J.; Baum, L. G. Galectin-1-mediated apoptosis in mycosis fungoides: The roles of CD7 and cell surface glycosylation. *Mod. Pathol.* **2003**, *16* (6), 543−551.
(57) Tsuboi, S.; Sutoh, M.; Hatakeyama, S.; Hiraoka, N.; Habuchi, T.; Horikawa, Y.; Hashimoto, Y.; Yoneyama, T.; Mori, K.; Koie, T.; Nakamura, T.; Saitoh, H.; Yamaya, K.; Funyu, T.; Fukuda, M.; Ohyama, C. A novel strategy for evasion of NK cell immunity by tumours expressing core2 O-glycans. *EMBO J.* **2011**, *30* (15), 3173−85.
(58) Tsuboi, S.; Hatakeyama, S.; Ohyama, C.; Fukuda, M. Two opposing roles of O-glycans in tumor metastasis. *Trends Mol. Med.* **2012**, *18* (4), 224−32.
(59) Tsuboi, S. Immunosuppressive Functions of Core2 O-Glycans against NK Immunity. *Trends Glycosci. Glycotechnol.* **2013**, *25* (143), 117−123.
(60) Tsuboi, S. Roles of Glycans in Immune Evasion from NK Immunity. In *Sugar Chains: Decoding the Functions of Glycans*, Suzuki, T.; Ohtsubo, K.; Taniguchi, N., Eds.; Springer: Tokyo, Japan, 2015; pp 177−188.
(61) Suzuki, Y.; Sutoh, M.; Hatakeyama, S.; Mori, K.; Yamamoto, H.; Koie, T.; Saitoh, H.; Yamaya, K.; Funyu, T.; Habuchi, T.; Arai, Y.; Fukuda, M.; Ohyama, C.; Tsuboi, S. MUC1 carrying core 2 O-glycans functions as a molecular shield against NK cell attack, promoting bladder tumor metastasis. *International journal of oncology* **2012**, *40* (6), 1831−1838.
(62) Okamoto, T.; Yoneyama, M. S.; Hatakeyama, S.; Mori, K.; Yamamoto, H.; Koie, T.; Saitoh, H.; Yamaya, K.; Funyu, T.; Fukuda, M.; Ohyama, C.; Tsuboi, S. Core2 O-glycan-expressing prostate cancer cells are resistant to NK cell immunity. *Mol. Med. Rep.* **2013**, *7* (2), 359−64.
(63) Van Rinsum, J.; Smets, L. A.; Van Rooy, H.; Van den Eijnden, D. H. Specific inhibition of human natural killer cell-mediated cytotoxicity by sialic acid and sialo-oligosaccharides. *Int. J. Cancer* **1986**, *38* (6), 915−22.
(64) Ogata, S.; Maimonis, P. J.; Itzkowitz, S. H. Mucins Bearing the Cancer-Associated Sialosyl-Tn Antigen Mediate Inhibition of Natural-Killer-Cell Cytotoxicity. *Cancer Res.* **1992**, *52* (17), 4741−4746.
(65) Hudak, J. E.; Canham, S. M.; Bertozzi, C. R. Glycocalyx engineering reveals a Siglec-based mechanism for NK cell immunoevasion. *Nat. Chem. Biol.* **2013**, *10* (1), 69−75.
(66) Recchi, M. A.; Hebbar, M.; Hornez, L.; Harduin-Lepers, A.; Peyrat, J. P.; Delannoy, P. Multiplex reverse transcription polymerase chain reaction assessment of sialyltransferase expression in human breast cancer. *Cancer Res.* **1998**, *58* (18), 4066−70.
(67) Lise, M.; Belluco, C.; Perera, S. P.; Patel, R.; Thomas, P.; Ganguly, A. Clinical correlations of alpha2,6-sialyltransferase expression in colorectal cancer patients. *Hybridoma* **2000**, *19* (4), 281−6.
(68) Moriwaki, K.; Noda, K.; Furukawa, Y.; Ohshima, K.; Uchiyama, A.; Nakagawa, T.; Taniguchi, N.; Daigo, Y.; Nakamura, Y.; Hayashi,

DOI: 10.1021/acs.jproteome.7b00672
J. Proteome Res. 2018, 17, 543−558

N.; Miyoshi, E. Deficiency of GMDS Leads to Escape from NK Cell-Mediated Tumor Surveillance Through Modulation of TRAIL Signaling. *Gastroenterology* **2009**, *137* (1), 188−198.
(69) Iwata, T.; Nishiyama, N.; Nagano, K.; Izumi, N.; Tsukioka, T.; Chung, K.; Hanada, S.; Inoue, K.; Kaji, M.; Suehiro, S. Preoperative serum value of sialyl Lewis X predicts pathological nodal extension and survival in patients with surgically treated small cell lung cancer. *J. Surg. Oncol.* **2012**, *105* (8), 818−24.
(70) Mizuguchi, S.; Inoue, K.; Iwata, T.; Nishida, T.; Izumi, N.; Tsukioka, T.; Nishiyama, N.; Uenishi, T.; Suehiro, S. High serum concentrations of sialyl Lewis(x) predict multilevel N2 disease in non-small-cell lung cancer. *Annals of Surgical Oncology* **2006**, *13* (7), 1010−1018.
(71) Mizuguchi, S.; Nishiyama, N.; Iwata, T.; Nishida, T.; Izumi, N.; Tsukioka, T.; Inoue, K.; Kameyama, M.; Suehiro, S. Clinical value of serum cytokeratin 19 fragment and sialyl-Lewis x in non-small cell lung cancer. *Ann. Thorac Surg* **2007**, *83* (1), 216−21.
(72) Mizuguchi, S.; Nishiyama, N.; Iwata, T.; Nishida, T.; Izumi, N.; Tsukioka, T.; Inoue, K.; Uenishi, T.; Wakasa, K.; Suehiro, S. Serum Sialyl Lewis(x) and cytokeratin 19 fragment as predictive factors for recurrence in patients with stage I non-small cell lung cancer. *Lung Cancer* **2007**, *58* (3), 369−375.
(73) Carbone, D. P.; Salmon, J. S.; Billheimer, D.; Chen, H.; Sandler, A.; Roder, H.; Roder, J.; Tsypin, M.; Herbst, R. S.; Tsao, A. S.; Tran, H. T.; Dang, T. P. VeriStrat (R) classifier for survival and time to progression in non-small cell lung cancer (NSCLC) patients treated with erlotinib and bevacizumab. *Lung Cancer* **2010**, *69* (3), 337−340.
(74) Akerley, W. L.; Arnaud, A. M.; Reddy, B.; Page, R. D. Impact of a multivariate serum-based proteomic test on physician treatment recommendations for advanced non-small-cell lung cancer. *Curr. Med. Res. Opin.* **2017**, *33* (6), 1091−1097.
(75) Grossi, F.; Rijavec, E.; Genova, C.; Barletta, G.; Biello, F.; Maggioni, C.; Burrafato, G.; Sini, C.; Dal Bello, M. G.; Meyer, K.; Roder, J.; Roder, H.; Grigorieva, J. Serum proteomic test in advanced non-squamous non-small cell lung cancer treated in first line with standard chemotherapy. *Br. J. Cancer* **2017**, *116* (1), 36−43.
(76) Milan, E.; Lazzari, C.; Anand, S.; Floriani, I.; Torri, V.; Sorlini, C.; Gregorc, V.; Bachi, A. SAA1 is over-expressed in plasma of non small cell lung cancer patients with poor outcome after treatment with epidermal growth factor receptor tyrosine-kinase inhibitors. *J. Proteomics* **2012**, *76*, 91−101.

DOI: 10.1021/acs.jproteome.7b00672
J. Proteome Res. 2018, 17, 543−558

Supporting Information

Stage Dependence, Cell-Origin Independence and Prognostic Capacity of Serum Glycan Fucosylation, β1-4 Branching, β1-6 Branching and α2-6 Sialylation in Cancer

Shadi Ferdosi [a, b], Douglas S. Rehder [b,‡], Paul Maranian [b], Erik P. Castle [c], Thai H. Ho [d], Harvey I. Pass [e], Daniel W. Cramer [f], Karen S. Anderson [b], Lei Fu [g], David E. C. Cole [g], Tao Le [h], Xifeng Wu [h], and Chad R. Borges [a, b, *]

[a] School of Molecular Sciences, Arizona State University, Tempe, AZ 85287

[b] Virginia G. Piper Center for Personalized Diagnostics, The Biodesign Institute at Arizona State University, Tempe, AZ 85287

[c] Department of Urology, Mayo Clinic, Phoenix, AZ 85054

[d] Division of Hematology and Medical Oncology, Mayo Clinic, Phoenix, AZ 85054

[e] Cardiothoracic Surgery, NYU Langone Medical Center, New York, NY 10016

[f] Obstetrics and Gynecology Epidemiology Center, Department of Obstetrics and Gynecology, Brigham and Women's Hospital, Boston, MA; and Department of Epidemiology, Harvard School of Public Health, Boston, MA

[g] Department of Clinical Pathology, Sunnybrook Health Sciences Centre and Department of Laboratory Medicine and Pathobiology, University of Toronto, Toronto, ON, Canada

[h] University of Texas MD Anderson Cancer Center, Houston, TX 77030

*Author to whom correspondence should be addressed: Chad R. Borges, The Biodesign Institute at Arizona State University, P.O. Box 876401, Tempe, AZ 85287. Tel 480-727-9928; email: chad.borges@asu.edu

‡Current address: Gilead Sciences, Inc. 4049 Avenida de la Plata Oceanside, CA 92056

Table of Contents

Table S1 (Page S-3): Basic clinical characteristics and n-values of the large lung cancer and certifiably healthy living kidney donors sample sets.

Table S2 (Page S-4): Impact of plasma and serum matrices on glycan node measurements.

Table S3 (Page S-5): Comparison of sodium heparin plasma to potassium EDTA plasma and serum matrices.

Table S4 (Page S-6): Statistically significant differences between cohorts within the large lung cancer study.

Table S5 (Page S-7): Stage-by-stage comparison of the top performing glycan nodes

Figure S1 (Page S-8): Univariate distributions and associated ROC curves for the top five-performing glycan nodes in the large lung cancer set when data were normalized to the sum of endogenous hexoses or HexNAcs.

Appendix S1 (Pages S-9 to S-15): Inclusion and exclusion criteria for certifiably healthy living kidney donors.

Ferdosi et al All Data.xlsm – Raw and normalized chromatographic peak areas for all clinical samples in this study

Table S1: Basic clinical characteristics and n-values of the large lung cancer and certifiably healthy living kidney donors sample sets.

		Certifiably Healthy Living Kidney Donors[a]	Large Lung Cancer Set: Controls	Large Lung Cancer Set: Cases
Age [b]		46.5 ± 13.5[c]	60.5 ± 9.9	60.7 ± 10.3
Gender	Female	17	76	76
	Male	13	123	123
Smoking Status	Never-Smoker	22	38	34
	Former Smoker	8	80	70
	Current Smoker	0	81	95
Staging	Stage I	N/A	N/A	20
	Stage II	N/A	N/A	20
	Stage III	N/A	N/A	81
	Stage IV	N/A	N/A	78
Tumor Histology	Adenocarcinoma	N/A	N/A	79
	Squamous Cell Carcinoma	N/A	N/A	80
	Small Cell Carcinoma	N/A	N/A	40

[a] These specimens were collected as part of a separate study, see Methods section for additional details

[b] Age in years ± S.D.

[c] Significantly different from Controls and Cases (Kruskal-Wallis with Dunn's posthoc test; $p < 0.0001$)

Table S2: Impact of plasma and serum matrices on glycan node measurements. Data were acquired from 21 healthy individuals from which 5 different plasma or serum matrices were collected at the same draw. Differences between matrices were evaluated by the Friedman test followed by Dunn's post hoc test; $p > 0.05$ (ns), $p < 0.05$ (*), $p < 0.01$ (**).

Glycan Node	K_2EDTA vs. K_3EDTA	K_2EDTA vs. Na EDTA	K_2EDTA vs. 3.8% Na Citrate	K_2EDTA vs. Serum	K_3EDTA vs. Na EDTA	K_3EDTA vs. 3.8% Na Citrate	K_3EDTA vs. Serum	Na EDTA vs. 3.8% Na Citrate	Na EDTA vs. Serum	3.8% Na Citrate vs. Serum
t-Fucose	ns	ns	ns	ns	ns	ns	ns	ns	ns	*
t-Gal	ns	ns	ns	ns	ns	ns	ns	ns	ns	ns
2-Man	ns	ns	ns	ns	ns	ns	ns	ns	ns	ns
4-Glc	ns	ns	ns	ns	ns	*	ns	ns	ns	ns
3-Gal	ns	ns	ns	ns	ns	ns	ns	ns	ns	ns
6-Gal	ns	ns	ns	ns	ns	ns	ns	ns	ns	ns
3,4-Gal	ns	ns	ns	ns	ns	ns	ns	ns	ns	ns
2,4-Man	ns	ns	ns	ns	ns	ns	ns	ns	ns	ns
2,6-Man	ns	ns	ns	ns	ns	ns	ns	ns	ns	ns
3,6-Man	ns	ns	ns	ns	ns	ns	ns	ns	ns	ns
3,6-Gal	ns	ns	ns	ns	ns	ns	ns	ns	ns	ns
3,4,6-Man	ns	ns	ns	ns	ns	*	ns	ns	ns	ns
t-GlcNAc	ns	ns	ns	ns	ns	ns	ns	ns	ns	ns
4-GlcNAc	ns	ns	ns	ns	ns	ns	ns	ns	ns	ns
3-GlcNAc	ns	ns	ns	ns	ns	ns	ns	ns	ns	ns
3-GalNAc	ns	ns	ns	ns	ns	ns	ns	ns	**	**
3,4-GlcNAc	ns	ns	ns	ns	ns	ns	ns	ns	ns	ns
4,6-GlcNAc	ns	ns	ns	ns	ns	ns	ns	ns	ns	ns
3,6-GalNAc	ns	ns	**	ns	ns	ns	ns	ns	ns	**

Table S3: Comparison of sodium heparin plasma to potassium EDTA plasma and serum matrices. Data were acquired from 6 replicate analyses (per matrix) of a matched set of samples taken from a single donor during one blood draw. Differences between matrices were evaluated by the Friedman test followed by Dunn's post hoc test; $p > 0.05$ (ns), $p < 0.05$ (*).

Glycan Node	Heparin vs. K_2EDTA	Heparin vs. Serum	K_2EDTA vs. Serum
t-Fucose	ns	ns	ns
t-Gal	ns	ns	ns
2-Man	ns	ns	ns
4-Glc	ns	ns	ns
3-Gal	ns	ns	ns
6-Gal	*	ns	ns
3,4-Gal	*	*	ns
2,4-Man	ns	ns	*
2,6-Man	ns	*	ns
3,6-Man	ns	ns	ns
3,6-Gal	ns	ns	ns
3,4,6-Man	ns	ns	ns
t-GlcNAc	ns	ns	ns
4-GlcNAc	ns	ns	ns
3-GlcNAc	ns	ns	ns
3-GalNAc	ns	ns	ns
3,4-GlcNAc	ns	*	ns
4,6-GlcNAc	ns	ns	ns
3,6-GalNAc	ns	ns	ns

Table S4: Statistically significant differences between cohorts within the large lung cancer study. Hexose data were normalized to the sum of endogenous hexoses and HexNAc data were normalized to the sum of endogenous HexNAcs.

Glycan Node [a,b,c]	C vs I	C vs. II	C vs. III	C vs. IV	I vs. II	I vs. III	I vs IV	II vs III	II vs IV	III vs IV
t-Fucose	ns	ns	ns	ns	ns	ns	ns	ns	ns	ns
t-Gal	ns	ns	dddd	dddd	ns	ns	ns	ns	ns	ns
2-Man	ns	ns	ns	ns	ns	ns	ns	ns	ns	ns
4-Glc	ns	ns	ns	ns	ns	ns	ns	ns	ns	ns
3-Gal	ns	ns	ns	ns	ns	ns	ns	ns	ns	ns
6-Gal	ns	ns	ii	ii	ns	ii	ii	ii	ii	ns
3,4-Gal	ns	i	ns	ns	ns	ns	ns	ns	ns	ns
2,4-Man	ns	ns	iiii	iiii	ns	ii	i	ns	ns	ns
2,6-Man	ns	ns	iii	iii	ns	i	i	i	ns	ns
3,6-Man	ns	ns	ns	ns	ns	ns	ns	ns	ns	ns
3,6-Gal	ns	ns	ns	ns	ns	ns	ns	ns	ns	ns
3,4,6-Man	ns	ns	d	dd	ns	d	d	ns	d	ns
t-GlcNAc	ns	ns	ns	ns	ns	ns	ns	ns	ns	ns
4-GlcNAc	ns	ns	ns	ns	ns	ns	ns	ns	ns	ns
3-GlcNAc	ns	ns	ns	ns	ns	ns	ns	ns	ns	ns
3-GalNAc	ns	ns	ddd	ddd	ns	ns	ns	ns	ns	ns
3,4-GlcNAc	ns	ns	iiii	iiii	ns	ns	ns	ns	ns	ns
4,6-GlcNAc	ns	ns	d	dd	ns	ns	ns	ns	ns	ns
3,6-GalNAc	ns	ns	dd	ddd	ns	ns	ns	ns	ns	ns

[a] Kruskal-Wallis test followed by Benjamini-Hochberg false discovery correction procedure where significance at the 95% confidence level is given by $p < 0.05$.

[b] “ns” indicates "not significant". “i” and “d” stand for “increased” or “decreased” in the clinically more-advanced cohort listed in the column header. i/d indicates $p < 0.05$; ii/dd indicates $p < 0.01$, iii/ddd indicates $p < 0.001$, iiii/dddd indicates $p < 0.0001$.

[c] CH: Certifiably Healthy, C: Controls, I: Stage I, II: Stage II, III: Stage III, IV: Stage IV

Table S5: Stage-by-stage comparison of the top performing glycan nodes. Comparisons are made for the large lung cancer set vs. other independent lung cancer sets (stages IV and I), ovarian (stage III) or prostate cancer (stage II). Actual ROC curves are shown in Fig. 4.

Stages	Glycan Feature	A: ROC AUC of Set A (Specified in Left Column) B: ROC AUC of Set B (Large Lung Cancer Set)	p-value of DeLong's test for two ROC curves [a]
Stage IV **Sample Sets Compared (See Table 1):** **Set A: Stage IV Lung Cancer** **Set B: Large Lung Cancer**	Terminal (Total) Fucosylation	A: 0.851 B: 0.841	0.907 (NS)
	α2-6 Sialylation	A: 0.949 B: 0.945	0.914 (NS)
	β1-4 Branching	A: 0.957 B: 0.953	0.937 (NS)
	β1-6 Branching	A: 0.938 B: 0.961	0.614 (NS)
	Outer-Arm Fucosylation	A: 0.826 B: 0.889	0.503 (NS)
Stage III **Sample Sets Compared (See Table 1):** **Set A: Serous Ovarian Cancer** **Set B: Large Lung Cancer**	Terminal (Total) Fucosylation	A: 0.794 B: 0.793	0.996 (NS)
	α2-6 Sialylation	A: 0.848 B: 0.907	0.179 (NS)
	β1-4 Branching	A: 0.829 B: 0.914	0.058 (NS)
	β1-6 Branching	A: 0.835 B: 0.928	0.035
	Outer-Arm Fucosylation	A: 0.870 B: 0.872	0.958 (NS)
Stage II **Sample Sets Compared (See Table 1):** **Set A: Prostate Cancer** **Set B: Large Lung Cancer**	Bisecting GlcNAc	A: 0.673 B: 0.576	0.253 (NS) [b]
	Terminal (Total) Fucosylation	A: 0.652 B: 0.560	0.298 (NS) [b]
	α2-6 Sialylation	A: 0.508 B: 0.571	0.507 (NS) [b]
	β1-4 Branching	A: 0.567 B: 0.583	0.872 (NS)
	β1-6 Branching	A: 0.587 B: 0.570	0.867 (NS) [b]
	Outer-Arm Fucosylation	A: 0.531 B: 0.615	0.346 (NS) [b]
Stage I **Sample Sets Compared (See Table 1):** **Set A: Stage I Lung Cancer** **Set B: Large Lung Cancer**	O-Glycan Core Branching	A: 0.634 B: 0.540	0.251 (NS) [b]
	Terminal (Total) Fucosylation	A: 0.573 B: 0.591	0.841 (NS)
	α2-6 Sialylation	A: 0.564 B: 0.553	0.893 (NS)
	β1-4 Branching	A: 0.555 B: 0.556	0.990 (NS)
	β1-6 Branching	A: 0.592 B: 0.503	0.243 (NS)
	Outer-Arm Fucosylation	A: 0.613 B: 0.566	0.540 (NS)

[a] NS indicates no significant difference between ROC curves.

[b] *p*-value is the result of Bootstrap test since the Delong's test should not be applied to ROC curves with opposite directionalities

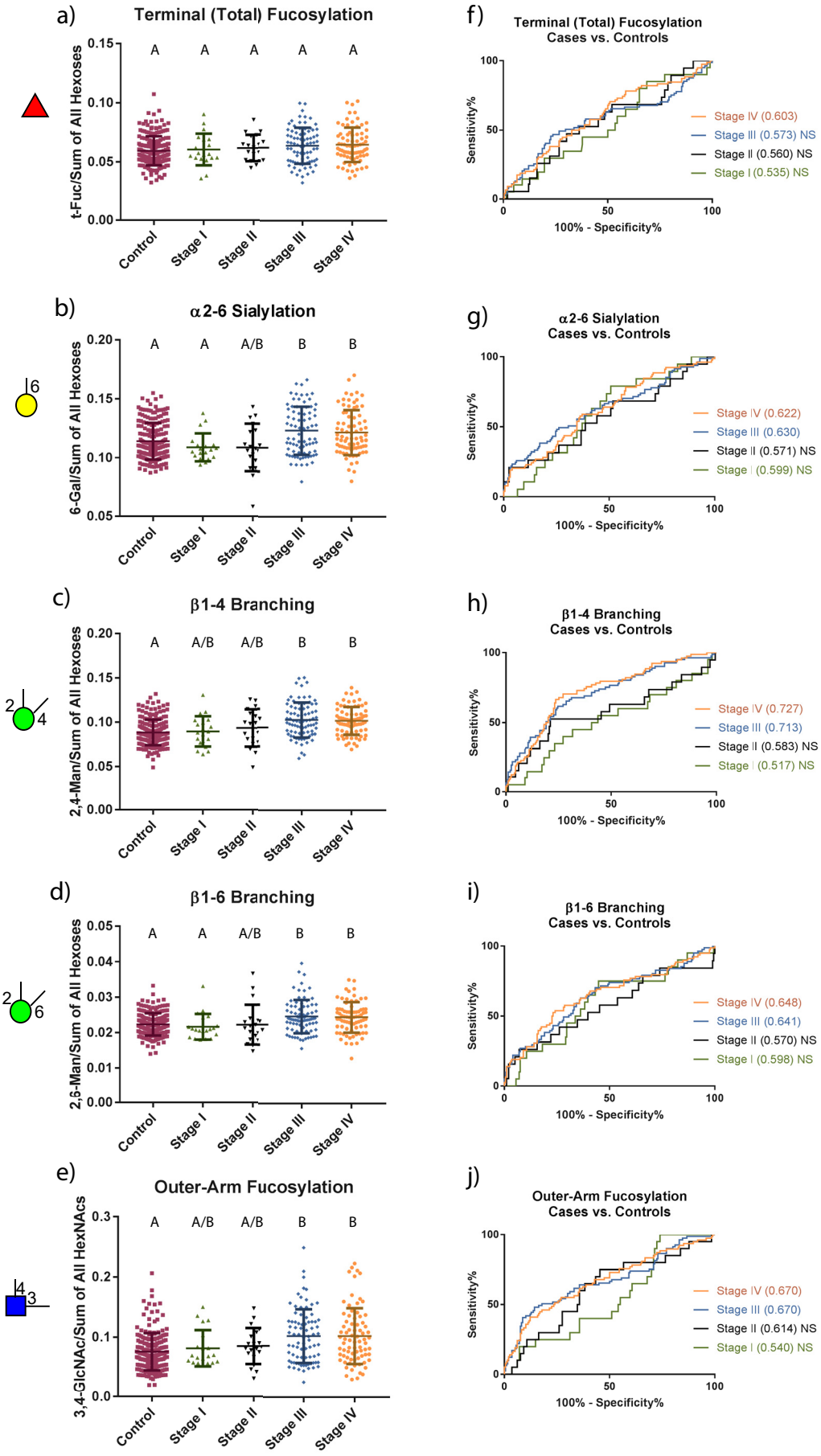

Figure S1: Univariate distributions and associated ROC curves for the top five-performing glycan nodes in the large lung cancer set when data were normalized to the sum of endogenous hexoses or HexNAcs. Letters above the data points in panels a-e indicate statistically significant differences between the five groups shown: any overlap in lettering between groups indicates a lack of significant difference between the groups (Kruskal-Wallis with Dunn's post hoc test). ROC curves for lung cancer cases (separated by stage) vs. controls are shown in panels f-j. ROC curve AUCs are provided in parenthesis next to the specified stages. "NS" next to ROC curve AUCs indicates that the ROC curve does not show a statistically significant difference between the two groups being compared. Glycan node symbol definitions are the same as in Fig. 1.

Inclusion and Exclusion Criteria for Certifiably Healthy Living Kidney Donors

Mayo Clinic Arizona Guidelines

Inclusion Criteria

All persons that wish to be considered as a potential living donor will be evaluated using the following criteria:

- Age
    - Between the ages of 18-70
    - Those above age 70 will be considered on a case-by-case basis
- BMI and Blood Glucose
    - Evaluation of Living Kidney Donor: BMI and Glucose Metabolism Guideline
        - Impaired Fasting Glucose (FBS > 100 and < 126) or IGT (2 hour BS > 140 and < 200) is a relative contraindication to donation. Patients with family history of diabetes, gestational diabetes and/or metabolic syndrome may be at higher risk than others for developing DM.
        - Prospective donors meeting these criteria require counseling about increased risk of developing DM and its consequences.
- Blood Pressure
    - All patients worked up at Mayo Clinic will complete either a 24 hour blood pressure monitor, a blood pressure taken on at least two different occasions, or overnight BP monitoring to be analyzed
    - Criteria for the diagnosis of Hypertension
        - Clinic or hypertensive therapy nurse blood pressure > 140/90 mm Hg
        - ABPM awake period (mean value) > 135/85 mm Hg
        - ABPM overall (mean value) > 130/80
    - Donor Selection
        - Normal Blood pressure acceptable as a donor
        - Hypertension may be acceptable if all met:
            1. Greater than age 40
            2. Caucasian

3. GFR meets Evaluation of Living Kidney Donor: GFR Protocol
4. Hypertension controlled with one drug + diuretic

- Kidney Function – GFR Standards
  - Evaluation of Living Kidney Donor: GFR Protocol
- Malignancy
  - Evaluation of the Living Kidney Donor: Donor Malignancy Guideline
- Crossmatch/ABO
  - Arizona: See Living Donors Blood Type, Subtype Determination Policy and ABO Verification for Living Donors Policy
  - Florida: See Living Donors Blood Type, Subtype Determination Policy and See ABO Verification for Living Donors Policy
  - Rochester: See ABO Blood Group and Other Vital Data Compatibility Verification Guideline
- Pulmonary Nodules
  - Evaluation of the Living Kidney Donor: Pulmonary Nodules Guideline
- Stones
  - Evaluation of the Living Kidney Donor: Donor Nephrolithiasis Guideline
- Microscopic Hematuria
  - Evaluation of the Living Kidney Donor: Donor with Microscopic Hematuria Guideline
- Polycystic Kidney Disease
  - Evaluation of the Living Donor: Polycystic Kidney Disease Guideline
- Psychiatric
  - Evaluation of the Living Donor: Psychiatric Evaluation policy
- Donor Coercion
  - Evaluation of the Living Donor: Coercion Guideline

Exclusion Criteria

- The transplant center may exclude a donor with any condition that, in the hospital's medical/ethical judgment, causes the donor to be unsuitable for organ donation.

- The transplant center will exclude all donors who meet any of the following exclusion criteria:
    - Is less than 18 years old
    - Is mentally incapable of making an informed decision
    - History of HIV
    - Infectious Disease that can be transmitted through transplantation
    - Active malignancy, or incompletely treated malignancy
    - High suspicion of donor coercion
    - High suspicion of illegal financial exchange between donor and recipient
    - Evidence of acute symptomatic infection (until resolved)
    - Uncontrolled diagnosable psychiatric conditions requiring treatment before donation, including any evidence of suicidality
    - Uncontrollable hypertension or history of hypertension with evidence of end organ damage
    - Diabetes mellitus
    - Consider on an individual basis, usually not accepted as donor
        - Non-Caucasian with hypertension
        - Other antihypertensive regimens
        - Family history of hypertensive kidney injury
        - Evidence of end organ damage such as Left Ventricular Hypertrophy (LVH)
        - Additional risk factors particularly active smoking

Additional Information Regarding Living Kidney Donor Selection

Donor Screening

- A potential donor will be screened by the living donor coordinator on the phone or by completing an electronic form.
- In addition, a social work interview is to be conducted for all potential donors if requested by the living donor coordinator.

- At that point, blood type and tissue typing will be obtained and reviewed by the donor team.
- If suitable, potential donor will be scheduled for an evaluation.

Donor Evaluation

Living donor candidate workups are valid for a duration of 18 months after being accepted at selection conference; thereafter, any repeat testing necessary will be determined by the evaluating team at the donor site after which the candidate will again be presented at selection conference.

Workup of the donor will include:

- Labs:
    - CBC with differential
    - PT/INR and PTT
    - Renal Profile (BUN, Creatinine, Electrolytes)
    - Fasting glucose and A1C
    - Liver function profile
    - Thyroid Stimulating Hormone
    - Fasting Lipid Profile
    - Serum protein electrophoresis for age >60
    - Oral glucose tolerance test for high risk patients per the Evaluation of Living Kidney Donor: BMI and Glucose Metabolism Guideline
    - HCG Quantitative blood (female < 55)
- Serologies:
    - See Infectious Disease Protocol
- Clearance Studies and 24 hour urine collection:
    - Spot micro albumin/creatinine ratio
    - Iothalamate GFR clearance and 24 hour creatinine clearance
- Urine tests:
    - Routine urinalysis
    - Midstream Gram stain and culture

- Urine microscopy
- Stone risk profile for any donor with history of nephrolithiasis per the Evaluation of Living Kidney Donor: Donor Nephrolithiasis Guideline

- Other tests:
  - Chest x-ray
  - EKG
  - Exercise Stress Echo (> 60 years or high cardiac risk) (>50 with hypertension or tobacco use) and/or dobutamine or nuclear stress test if clinically appropriate (may consider for younger patients on case to case basis)
  - Screening for Autosomal Dominant Polycystic Kidney Disease (ADPKD) (for related donors of ADPKD recipient)
    - Per the Evaluation of Living Kidney Donor: Polycystic Disease Guideline
  - CT angiography: renal protocol to determine:
    - Whether the kidneys are of equal size
    - If the kidneys have masses, cysts, or stones
    - If the kidneys have other anatomical defects
    - Which kidney is more anatomically suited for transplant
- Cancer screening per American Cancer Society (ACS) guidelines:
  - Mammogram (females ≥40 or if h/o breast cancer in pre-menopausal 1st degree relative)
  - Cologuard (≥50 or family history) - first tier for low-risk patients
  - Females should have a Pap smear every three years, provided most recent Pap smear was normal. If most recent Pap smear was not normal, follow-up should be according to the recommendations of the GYN service.
  - PSA
    - Age 50 for men who are at average risk of prostate cancer and are expected to live at least 10 more years
    - Age 45 for men at high risk of developing prostate cancer. This includes African Americans and men who have a first-degree relative (father, brother, or son) diagnosed with prostate cancer at an early age (younger than age 65)

        - Age 40 for men at even higher risk (those with more than one first-degree relative who had prostate cancer at an early age)
    - Low-Dose CT scan for those at high risk for lung cancer (those who meet all of the below):
        - 55 to 74 years of age
        - Have at least a 30 pack-year smoking history AND are either:
            - Still smoking OR
            - Have quit within the last 15 years

Note: A pack-year is the number of cigarette packs smoked each day multiplied by the number of years a person has smoked. Someone who smoked a pack of cigarettes per day for 30 years has a 30 pack-year smoking history, as does someone who smoked 2 packs a day for 15 years.

- Consultations:
    - Nephrology (different physician from recipient if possible)
    - Living Donor Nurse Coordinator
    - Social Services (different from recipient social worker if possible)
    - Nutrition
    - Pharmacy
    - Transplant Surgeon/Urologist
    - Consider Transplant Psychiatrist/Clinical Psychology Specialist
    - Independent Living Donor Advocate
- Any additional tests, procedures, consults or biopsies needed to determine their candidacy is a part of the donor evaluation until the donor is ruled out as a donor

Selection Conference

- The final decision to proceed with donation made at the Selection Conference, which may include the following multi-disciplinary team members: transplant surgeons, nephrologists, independent living donor advocate, psychiatrist, social worker, dietitian, pharmacists, financial services and nursing personnel.
- Cases will be presented to the Selection Committee once all appointments completed and all results available.

- Results of testing and assessments will be reviewed by the multi-disciplinary Selection Committee, providing an opportunity for all members to raise concerns and discuss any issues regarding the donor's suitability.
- The living donor’s suitability for donation will be thoroughly documented in the donor’s medical record
- The decision of the committee will be documented in the donor's medical record and communicated to potential donor by a member of the multidisciplinary team.
- Any exceptions to the selection criteria must be approved by the Living Kidney Donor Selection Committee & the reasons for it thoroughly documented in the patient’s medical record